cmgh
CELLULAR AND MOLECULAR GASTROENTEROLOGY AND HEPATOLOGY

ORIGINAL RESEARCH

Elevated Bile Acids Induce Circadian Rhythm Sleep Disorders in Chronic Liver Diseases

Lan Zhou,[1,2,*] Min Yan,[1,2,*] Qin Luo,[1,2] Wen Qiu,[1,2] Yu-Ru Guo,[1,2] Xiao-Qing Guo,[3] Hong-Bin Yu,[4] Jing-Ru Huo,[1,2] Yan-Lin Feng,[1,2] De-Ping Wang,[1,2] Teng Sun,[1,2] Kai-Fang Wang,[1,5] Jian-Yun Shi,[1,2] Xuan Shang,[1,2] Mei-Na Wu,[1,2] Lin Wang,[6] and Ji-Min Cao[1,2]

[1]Key Laboratory of Cellular Physiology, Shanxi Medical University, Ministry of Education, Taiyuan, China; [2]Department of Physiology, Shanxi Medical University, Taiyuan, China; [3]Department of Hepatology, Taiyuan Third People's Hospital, Taiyuan, China; [4]Department of General Surgery, Cancer Hospital of Shanxi Medical University, Shanxi Provincial Cancer Hospital, Taiyuan, China; [5]Department of Cardiology, The First Hospital and First College of Clinical Medicine, Shanxi Medical University, Taiyuan, China; and [6]Department of Physiology, Institute of Basic Medical Sciences, Chinese Academy of Medical Sciences, School of Basic Medicine, Peking Union Medical College, Beijing, China

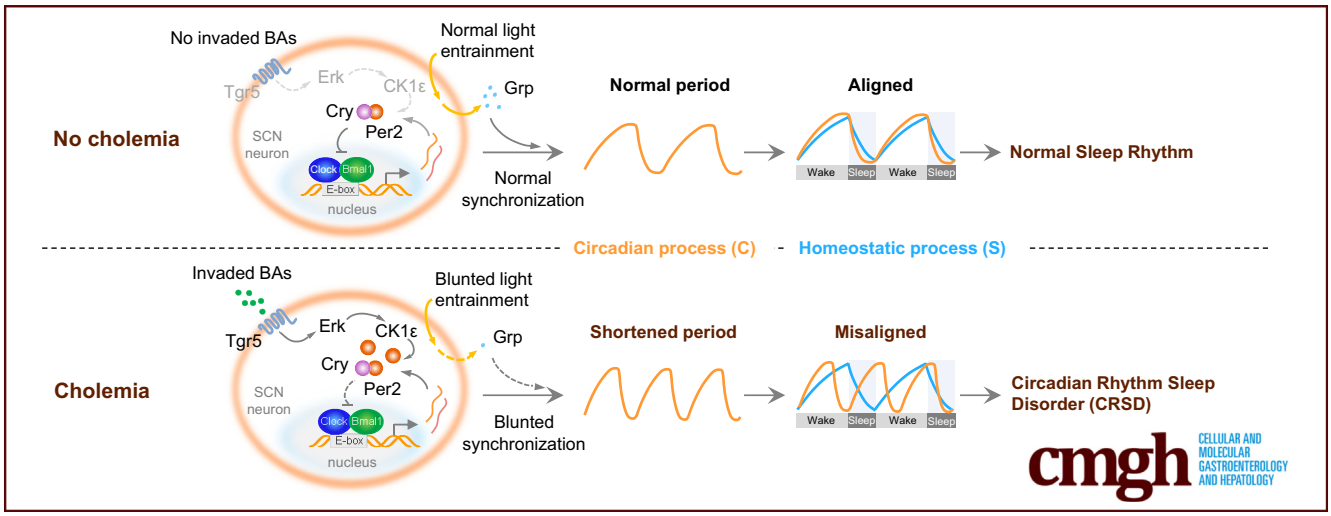

SUMMARY

In chronic liver diseases, circadian rhythm sleep disorders were correlated with elevated bile acid levels. Bile acids activated Tgr5 in suprachiasmatic nucleus and reduced Per2 nuclear import, causing shorter circadian period, blunted light entrainment via Grp, and impaired sleep processes.

BACKGROUND & AIMS: Sleep disorders (SDs) are common in chronic liver diseases (CLDs). Some SDs arise from impaired internal clock and are, hence, circadian rhythm SDs (CRSDs). Bile acids (BAs), whose levels are increased in many CLDs, reciprocally interact with circadian rhythm. This study explores the mechanisms underlying CRSDs in CLDs and novel therapies.

METHODS: We monitored the sleep of patients with CLD using actigraphic watch and established male mouse cholemia models by feeding with BA or bile duct ligation. Sleep-wake cycle and circadian rhythm were analyzed by electroencephalogram-electromyography and locomotor wheel-running experiments.

RESULTS: Patients with CLD showed CRSD-like phenotypes including increased night activity and early awakening, which were strongly correlated with increased BA levels (ie, cholemia). CRSDs, including shortened circadian period, were recapitulated in 2 cholemic mouse models. Mechanistically, elevated BAs in the suprachiasmatic nucleus (SCN) activated BA receptor Takeda G protein-coupled receptor 5 (Tgr5), which, in turn, increased the level and phosphorylation of Period2 (Per2), a master rhythm regulator, through extracellular signal-regulated kinase (Erk) and casein kinase 1ε (CK1ε). Per2 phosphorylation inhibited its nuclear import, which would release its transcriptional inhibition and expedite the circadian cycle. Cholemia also blunted the light entrainment response and light-induced phase change of SCN mediated by the neurons expressing gastrin releasing peptide through Tgr5-Per2 axis. BA sequestrant or CK1 inhibitor reversed the CRSDs in cholemic mice by restoring Per2 distribution.

CONCLUSIONS: Cholemia is a major risk factor for CRSDs in CLDs and, hence, a promising target in future clinical study. *(Cell Mol Gastroenterol Hepatol 2025;19:101439; https://doi.org/10.1016/j.jcmgh.2024.101439)*

Keywords: Bile Acid; Chronic Liver Disease; Circadian Rhythm Sleep Disorder; Takeda G Protein-Coupled Receptor 5.

Sleep disruption is prevalent in many chronic liver diseases (CLDs), including hepatitis B (HB),[1–3] nonalcoholic liver cirrhosis (NALC),[4,5] hepatic encephalopathy (HE),[6] and primary biliary cirrhosis (PBC).[7,8] The phenotypes and etiology of sleep disorders (SDs) in CLDs are complex and cannot be fully attributable to the neurotoxicity arising from HE.[9,10] Some patients with CLD exhibits the characteristics of circadian rhythm sleep disorder (CRSD), such as the greater sleep latency, shorter sleep duration, and dampened rest-activity rhythms.[6,11] A two-process model posits that sleep is regulated by sleep-wake-dependent homeostatic process (S) and history-independent circadian process (C), which seem to selectively affect the slow-wave activity (SWA) fraction of the non-rapid eye movement (NREM) sleep and rapid eye movement (REM) sleep, respectively.[12,13] To date, the mechanisms underlying SDs in CLDs are unknown, leading to limited treatment options and poor quality of life in these patients.

In mammals, numerous physiological and behavioral processes including the sleep-wake cycle exhibit a ∼24-hour circadian rhythm. The mammalian circadian system consists of a master central clock, the suprachiasmatic nucleus (SCN) in the hypothalamus, which is the principal pacemaker and entrainable to the alternating day/night environment, and the peripheral clocks in other tissues, which synchronize and coordinate with SCN. At the molecular level, the cell-autonomous circadian oscillator is generated by several transcription-translation negative feedback loops.[14] In the primary feedback loop, 2 transcription factors, circadian locomotor output cycles kaput (CLOCK) and brain and muscle ARNT-like 1 (BMAL1) form a complex that activates the transcription of *PERIOD* genes (*PER1, PER2*, and *PER3*) and *CRYPTOCHROME* genes (*CRY1* and *CRY2*). The translated PER and CRY proteins then form a complex in the cytosol and are translocated to the nucleus to repress their own transcription by inhibiting the CLOCK/BMAL1 complex. In the meantime, PER and CRY are degraded by the ubiquitin-proteasome system such that the reduced levels of PER and CRY eventually release CLOCK/BMAL1 from inhibiting *PER* and *CRY* transcription, thus allowing another circadian cycle to begin.

PERIOD2 (PER2) is a master rhythm regulator in this clock circuit.[14] The level of PER2 over a day and the timing of PER2 nuclear accumulation set the period and phase of the circadian clock.[15,16] Global knockout of *Per2* in mice yielded a shortened circadian period.[15] Casein kinase 1δ/ε (CK1δ/ε) phosphorylates PER2, which affects its stability and nuclear translocation. For example, phosphorylation of PER2 at Ser478 leads to PER2 degradation, and PER2-S478A mutation lengthens the circadian period.[15,17,18] External light can also induce *Per2* transcription, which influences the phase of circadian rhythm.[19,20] In general, CRSDs can arise from an impaired internal clock and/or misalignment between the internal clock and the external environment.[21] Conceivably, PER2 and the factors affecting PER2 could play a critical role in CRSDs.

Bile acids (BAs), which are synthesized in the liver, function not only as detergents to assist lipid absorption but also as signaling molecules to regulate a wide range of physiological and pathophysiological processes. The synthesis and excretion of BAs is an essential function of the liver, which are often compromised in CLDs. In cholestasis, the compromised biliary secretion of BAs results in the accumulation of BAs in the liver and blood (ie, cholemia) via retrograde transport into the sinusoidal blood and the systemic circulation. In PBC, the rise of serum and liver BAs was reported to correlate with disease severity and progression.[22] Circadian rhythm and BA metabolism crosstalk at multiple levels.[23,24] For example, BA synthesis and transport are controlled by both the central and liver clocks.[23,25] Disrupted BA homeostasis or other metabolism such as hyperlipidemia could also change central circadian rhythms.[26] It is unclear if BAs, whose blood concentration fluctuates during the circadian cycle and fast-feeding cycle, directly regulate SCN. This study sought to explore the mechanisms underlying the SDs and especially the CRSDs in CLD.

In this study, we first noticed that there were 2 groups of patients in each CLD, characterized by normal and high levels of serum total BA (TBA), which we referred to as noncholemia and cholemia patients. After analyzing their sleep parameters and clinicodemographic data, we

***Authors share co-first authorship.**

Abbreviations used in this paper: **AAV, adeno-associated virus; ACF, artificial cerebrospinal fluid; ANOVA, analysis of variance; AP, anteroposterior; AVP, arginine vasopressin; BA, bile acid; BBB, blood-brain barrier; BDL, bile duct ligation; BMAL1, brain and muscle ARNT-like 1; BSA, bovine serum albumin; CA, cholic acid; CDCA, chenodeoxycholine acid; CHO, cholestyramine; CK1δ/ε, casein kinase 1δ/ε; CLD, chronic liver disease; CLOCK, circadian locomotor output cycles kaput; CRSD, circadian rhythm sleep disorder; CRY, CRYPTOCHROME; DCA, deoxycholic acid; DD, constant darkness; DHCA, dihydrocaffeic acid; DMEM, Dulbecco modified Eagle medium; EEG, electroencephalogram; EMG, electromyogram; ERK, extracellular signal-regulated kinase; FBS, fetal bovine serum; FI, fragmentation index; FXR, farnesoid X receptor; GCA, glycocholic acid; GDCA, glycodeoxycholic acid; GLCA, glycolithocholic acid; GRP, gastrin-releasing peptide; GUDCA, glycoursodeoxycholic acid; HB, hepatitis B; HBC, hepatitis B cirrhosis; HE, hepatic encephalopathy; LCA, lithocholic acid; LD, light-dark; MI, movement index; ML, medio-lateral; MS/MS, tandem mass spectrometry; NALC, nonalcoholic liver cirrhosis; ND, normal diet; NREM, non-rapid eye movement; OA, oleanolic acid; OPLS-DA, orthogonal partial least squares discriminant analysis; PBC, primary biliary cirrhosis; PBS, phosphate-buffered saline; PER, PERIOD; PER2, PERIOD2; p-Erk, phosphorylated Erk; PXR, preganane X receptor; REM, rapid eye movement; RNAi, RNA interference; RT-PCR, reverse transcription polymerase chain reaction; SCN, suprachiasmatic nucleus; SD, sleep disorder; SEM, standard error of the mean; SFI, sleep fragmentation index; shRNA, short hairpin RNA; siRNA, small interfering RNA; SWA, slow-wave activity; TBA, total bile acid; TBIL, total bilirubin; TCA, taurocholic acid; TCDCA, taurochenodeoxycholic acid; TGR5, Takeda G protein-coupled receptor 5; TMCA, tauro-muricholic acid; TRPA1, transient receptor potential ankyrin 1; TST, total sleep time; TUDCA, tauroursodeoxycholic acid; UDCA, ursodeoxycholic acid; VDR, vitamin D receptor; VIP, vasoactive intestinal peptide; WASO, wake after sleep onset; WT, wild-type.**

Most current article

2352-345X
https://doi.org/10.1016/j.jcmgh.2024.101439

identified the TBA level as a major risk factor strongly correlated with the CRSD-like symptoms. Next, we validated the role of BAs in CRSDs and circadian rhythm regulation using mouse cholemic models and explored the underlying mechanisms and novel therapies.

Results

Cholemia is a Major Risk Factor for SDs in Patients With CLD

We first noticed that the patients with CLD suffered differential degrees of sleep disruption and then screened their clinicodemographic data to identify any potential risk factors. The patients with CLD were classified into 2 groups based on their levels of TBA and total bilirubin (TBIL): a low TBA, low TBIL group and a high TBA, high TBIL group, which indicated differential levels of cholestasis in these patients. Based on their TBA level, we named them the noncholemia (TBA $\leq$10 μmol/L) and cholemia (TBA $>$10 μmol/L) groups (Table 1). No significant distinction was found among other clinicodemographic criteria.

We then analyzed the sleep parameters of these patients using actigraphic watch (Figure 1*A*). Compared with the noncholemia group, the cholemic patients with CLD exhibited significantly advanced out-bed time, shorter total sleep time (TST), longer wake after sleep onset (WASO), and greater sleep fragmentation index (SFI) (Figure 1*A*; Table 1). These sleep parameters were correlated with TBA levels but not with the levels of other metabolites or clinicodemographic data (Table 2). The out-bed time was also associated with the level of TBIL. In the patients with the same CLD, shorter TST, longer WASO, and greater SFI were also seen in the cholemia group, as compared with the noncholemia group (Figure 1*A*–*C and E*). Despite no uniform difference in the sleep and wake onset time, the cholemic patients from every CLD type exhibited

Table 1. Clinical Characteristics and Actigraphic Sleep Parameters of CLD Patients With or Without Cholemia

	No cholemia (n = 29)	Cholemia (n = 31)	*P* value
Group characteristics			
Male/female	17/12	17/14	.459
Age, *years*	54 (42–62)	54 (41–62)	.900
Diagnosis			.988
HB	9	10	
HBC	7	7	
PPBC	6	6	
NALC	7	8	
Stage			.848
HB/heavy	9	10	
Cirrhosis/compensated stage 1	3	1	
Cirrhosis/compensated stage 2	6	8	
Cirrhosis/decompensated stage 3	9	9	
Cirrhosis/decompensated stage 4	2	3	
Plasma tests			
TBA, *μmol/L*	5.80 (4.20–7.65)	118.5 (64.00–223.00)	< .001
TBIL, *μmol/L*	13.50 (9.10–16.85)	84.70 (42.10–140.45)	< .001
ALT, *U/L*	53.00 (31.00–74.50)	53.00 (46.00–86.00)	.287
AST, *U/L*	44.00 (35.50–76.00)	66.00 (44.00–91.00)	.080
UREA, *mmol/L*	4.80 (3.25–5.10)	4.20 (3.70–4.80)	.161
CRE, *μmol/L*	56.00 (41.00–61.00)	49.00 (40.00–55.00)	.032
TG, *mmol/L*	1.38 (0.97–2.19)	1.53 (1.06–1.87)	.923
TC, *mmol/L*	4.76 (3.84–5.16)	4.59 (4.12–5.26)	.888
HGB, *g/L*	129 (112–138)	125 (108–132)	.164
PLT, $\times 10^9$/L	118 (106–130)	121 (108–129)	.994
PT, *s*	13.80 (12.70–14.40)	13.90 (13.40–14.90)	.257
FIB, *g/L*	1.63 (1.41–1.78)	1.58 (1.43–1.75)	.559
TP, *g/L*	73.00 (62.50–79.00)	72.00 (62.00–77.00)	.441
AMM, *μmol/L*	21.00 (18.50–24.50)	24.00 (18.00–28.00)	.163
Actigraphic sleep parameters			
Sleep onset	22:47 (22:34–23:07)	22:46 (22:27–23:19)	.96
Out bed	6:29 (6:18–6:43)	5:40 (5:19–5:57)	< .001
TST, *minutes*	426.33 (407.34–435.50)	348.33 (337.33–381.67)	< .001
WASO, *minutes*	43.33 (36.17–51.67)	63.33 (56.67–76.67)	< .001
SFI	31.34 (26.91–33.32)	36.19 (33.66–39.52)	< .001

Note: Data are presented as number or median (quartile 1–quartile 3).
ALT, Alanine aminotransferase; AMM, blood ammonia; AST, aspartate aminotransferase; CLD, chronic liver diseases; CRE, creatinine; FIB, fibrinogen; HB, hepatitis B; HBC, hepatitis B cirrhosis; HGB, hemoglobin; NALC, nonalcoholic liver cirrhosis; PBC, primary biliary cirrhosis; PLT, platelet; PT, prothrombin time; SFI, sleep fragmentation index; TBA, total bile acid; Tbil, total bilirubin; TC, cholestenone; TG, triglyceride; TP, total protein; TST, total sleep time; UREA, Urea nitrogen; WASO, wake after sleep onset.

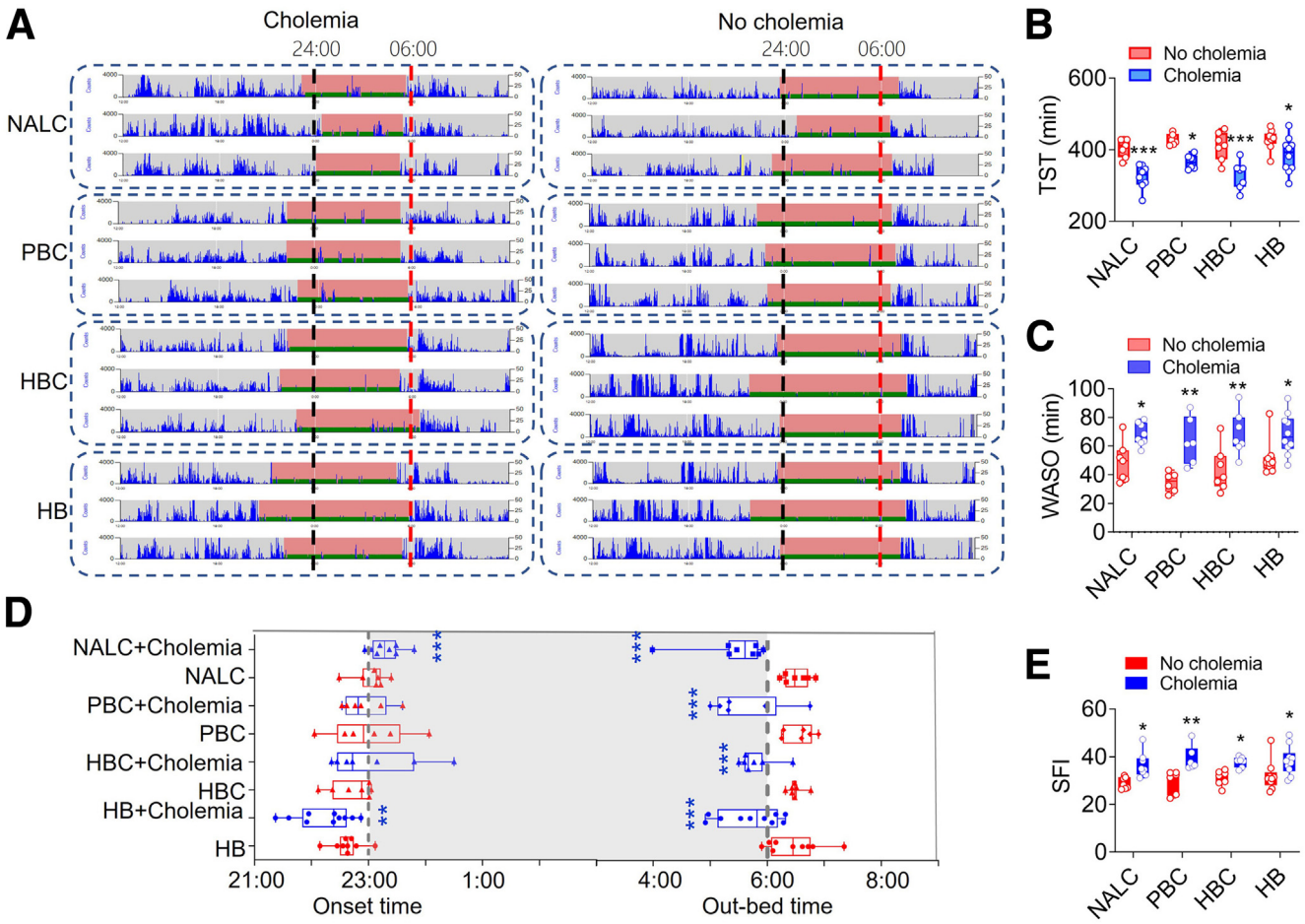

Figure 1. Actigraphic sleep parameters in CLD patients with or without cholemia. (*A*) Representative actograms for 3 consecutive days of 1 cholemic and 1 noncholemic patient with one of the four CLDs: NALC, HB, HBC, and PBC. *Blue bars* indicate activity with the same scale for each actogram. *Black dotted vertical lines* indicate 24:00/00:00, *red dotted vertical lines* denote 06:00, and *red areas* represent sleep duration. Note that patients with CLD and cholemia woke earlier (before 06:00) and had shortened sleep duration compared with those without cholemia (after 06:00 or even later). (*B*) TST. (*C*) WASO. (*D*) Sleep onset time and out-bed time. (*E*) SFI. N = 60 (NALC, n = 15; HB, n = 19; HBC, n = 14; and PBC, n = 12). Mean ± SEM, paired 2-tailed *t*-test. **P* < .05; ***P* < .01; ****P* < .001.

significantly advanced wake time, whereas delayed and advanced sleep onset was seen in the cholemic patients with NALC and HB (Figure 1*D*; Table 3).

These results demonstrate that the elevated BA level is a major, if not the only, risk factor for SDs in CLDs. The shorter sleep duration and phase changes of the cholemic patients with CLD are characteristic of the impairment of internal clock and failure of the internal clock to align with the external light in CRSDs. The blood count, procalcitonin, and C-reactive protein test results showed no significant difference between the noncholemic and cholemic patients with CLD (Table 4), suggesting that inflammation was not increased in the cholemic patients with CLD and thus was not a confounding factor in our study.

Cholemic Mice Exhibit CRSD-like Phenotypes

To investigate whether elevated BAs are sufficient to induce CRSD phenotypes, we created 2 mouse cholemic models by feeding with excess BA or bile duct ligation (BDL). Although BA feeding allows direct examination of the effect of BA on CRSDs, BDL mimics cholestasis but has additional pathologies besides cholemia. We first analyzed the wheel-running activities of these mice at constant darkness (DD), which is a classic condition to characterize the endogenous circadian rhythm (Figure 2*A and B*). The effects of 4 different BAs were compared, cholic acid (CA), chenodeoxycholic acid (CDCA), lithocholic acid (LCA), and ursodeoxycholic acid (UDCA). Notably, the circadian periods of the BA-fed mice except the UDCA-fed mice were much shorter than those of the normal diet (ND)-fed mice (Figure 2*A and C*). The paradoxical effect of UDCA is not surprising, as UDCA is a choleretic BA rather than a cholestatic BA.[27] No statistical difference was found in the phase shift between BA-fed mice and ND-fed mice under the DD condition (Figure 2*A and D*). The free-running period of the BDL mice at DD was also significantly shorter than that of the sham-operated mice (Figure 2*B and F*), and BDL mice also exhibited a phase delay (Figure 2*B and G*). In addition, when comparing with the ND-fed mice or sham-operated mice, the wheel-running

Table 2. Correlation of Demographic and Plasma Biochemical Parameters With Sleep Disorders in CLD Patients

		Sleep onset	Out bed	TST	WASO	SFI
Gender	β	−0.119	0.138	−0.039	−0.049	0.124
	P	.406	.218	.739	.685	.362
Age	β	−0.024	0.166	−0.155	−0.097	0.049
	P	.862	.127	.179	.403	.708
Diagnosis	β	0.475	−0.202	−0.187	0.187	−0.101
	P	.022	.200	.264	.269	.580
Stage	β	0.144	0.189	−0.122	−0.333	−0.032
	P	.509	.267	.501	.073	.872
TBA	β	−0.164	−1.007	−0.567	0.710	0.452
	P	.472	< .001	.004	.001	.037
TBIL	β	−0.312	−0.356	−0.160	−0.235	0.052
	P	.150	.038	.370	.196	.801
ALT	β	−0.100	0.028	−0.037	0.63	0.090
	P	.553	.833	.789	.654	.570
AST	β	−0.640	−0.053	−0.23	−0.072	−0.010
	P	.715	.698	.869	.627	.953
UREA	β	−0.089	−0.300	0.000	0.295	0.118
	P	.558	.803	.999	.024	.438
CRE	β	−0.184	−0.300	0.235	0.066	0.360
	P	.303	.827	.117	.659	.051
TG	β	−0.193	−0.163	−0.171	0.208	−0.013
	P	.196	.162	.167	.098	.925
TC	β	−0.025	0.027	0.109	0.128	−0.112
	P	.871	.821	.392	.320	.436
HGB	β	−0.091	−0.130	−0.002	0.250	0.310
	P	.589	.322	.986	.082	.054
PLT	β	0.112	0.124	−0.089	−0.026	−0.118
	P	.462	.298	.480	.841	.408
PT	β	0.011	−0.271	−0.143	0.023	−0.038
	P	.945	.128	.262	.860	.793
FIB	β	−0.072	0.145	0.206	−0.243	−0.203
	P	.641	.234	.115	.068	.178
TP	β	0.273	0.112	0.057	−0.098	−0.361
	P	.138	.433	.705	.521	.051
AMM	β	0.026	0.058	−0.129	0.036	−0.190
	P	.856	.607	.282	.766	.061

Note: β, standard regression coefficient; *P*, *P* value derived from multivariate linear regression analysis.
ALT, Alanine aminotransferase; AMM, blood ammonia; AST, aspartate aminotransferase; CLD, chronic liver diseases; CRE, creatinine; FIB, fibrinogen; HGB, hemoglobin; PLT, platelet; PT, prothrombin time; SFI, sleep fragmentation index; TBA, total bile acid; TBIL, total bilirubin; TC, cholestenone; TG, triglyceride; TP, total protein; TST, total sleep time; UREA, Urea nitrogen; WASO, wake after sleep onset.

activities of LCA-fed mice (Figure 2*E*) and BDL mice (Figure 2*H*) were markedly reduced, which may reflect the strong hydrophobicity and hence toxicity of LCA and a broad range of pathological conditions in the BDL model.[28]

We then examined BA's impact on circadian rhythm in mice exposed to the regular light-dark (LD) 12:12 photoperiod. To examine the dose dependence of BA and light, the mice were fed with increasing amounts of CA and were exposed to increasingly luminous environments (Figure 2*I*−*T*). Their wheel-running data showed that, under the 100 lux light condition, there was no significant difference in the circadian periods, wheel revolutions, and rest/activity durations between the 0.1% CA-fed mice and ND-fed mice (Figure 2*I, J, O, and P*). By contrast, the wheel-running period of 0.2% CA-fed mice was significantly shorter than that of the ND-fed mice in the first week of CA supplementation, suggesting 0.2% as the appropriate concentration to induce rhythmic changes (Figure 2*K and O*). During the second week of continuous feeding with 0.2% CA, the wake-up time of the mice did not further advance and neither did return to the normal wake-up time (Figure 2*K*). The 0.2% CA-fed mice exhibited substantially shortened rest duration (ie, more running activities) in the daytime (Figure 2*Q and R*), greater onset phase angle (Figure 2*S*), and greater light/dark activity ratio in the 24-hour cycle (Figure 2*U*), when compared with the ND-fed mice. Thus, the 0.2% CA-fed mice exposed to light of

Table 3. Actigraphic Sleep Parameters of Patients With Different CLDs

	NALC (n = 15)	PBC (n = 12)	HBC (n = 14)	HB (n = 19)	*P* value
Sleep onset time	23:10 (23:03–23:24)	22:49 (22:36–23:21)	22:48 (22:26– 23:05)	22:33 (22:09–22:42)	< .001
Out bed time	5:56 (5:28–6:29)	6:16 (5:19–6:43)	6:23 (5:39–6:29)	6:06 (5:42–6:27)	.586
TST, *minutes*	358.67 (322.67–411.67)	402.67 (357.75–425.58)	360.67 (334.50–415.33)	412.33 (367.33–432.67)	.126
WASO, *minutes*	57.00 (49.67–73.33)	44.00 (33.92–61.83)	56.33 (37.58–72.58)	53.33 (46.67–69.0)	.384
SFI	32.16 (28.24–35.00)	34.42 (31.64–37.23)	33.97 (33.06–38.00)	31.73 (30.03– 38.25)	.616

Note: Data are presented as median (quartile 1−quartile 3).
CLD, Chronic liver disease; HB, hepatitis B; HBC, hepatitis B cirrhosis; NALC, nonalcoholic liver cirrhosis; PBC, primary biliary cirrhosis; SFI, sleep fragmentation index; TST, total sleep time; WASO, wake after sleep onset.

normal intensity woke up 3 to 4 hours earlier than the ND-fed mice with a shorter sleep time.

Under the 200 lux condition, there was no significant difference in the circadian period between the 0.2% CA-fed mice and the ND-fed mice, suggesting that bright light acted as a stronger entraining signal and masked the rhythm-altering effect of CA (Figure 2*L*). Meanwhile, the 0.2% CA-fed mice exposed to 200 lux exhibited greater offset phase angle difference (Figure 2*T*). Under the same 200 lux condition, the 0.3% CA-fed mice did not follow the 24-hour LD cycle anymore and started to free run, suggesting that increased BAs exerted a bigger impact on the internal clock and overcame the masking effect of light (Figure 2*M and O*). 0.3% CA feeding also led to reduced rest duration and increased activity duration in the light phase (Figure 2*P and R*). Under this condition, reversing to the ND could not restore the normal wheel-running activity, suggesting a lasting effect induced by a higher level of BAs. When the light lumen was further increased to 300 lux, the brighter light again exerted a greater 'masking' effect and reversed the free-running induced by 0.3% CA (Figure 2*N and O*). It should be noted that the total wheel revolutions of the 0.3% CA-fed mice were markedly reduced (Figure 2*Q*), indicating the potential toxicity of 0.3% CA. These results confirm that BAs induce CRSD-like behaviors in a dose-dependent manner in cholemic mice. Timed bright light exposure, which has been widely used to reestablish a healthy shift in the treatment of patients with CRSD,[29] can mask the CA-induced rhythmic changes in cholemic mice.

Sleep Patterns of Cholemic Mice Were Consistent With CRSDs

To confirm that the locomotor activities indeed reflect sleep and wakefulness, we examined the electroencephalogram (EEG)/electromyogram (EMG) signals, which are the golden standard for sleep studies, in the control and CA-fed mice (Figure 3). The EMG signals were almost entirely restricted to the night, during which time the nocturnal rodents are awake and active. Conversely, the EEG signals were stronger during the daytime and dampened during the night (Figure 3*A and D−F*). Notably, the REM sleep, which is controlled by process C, was almost absent in the night/dark and exclusively restricted to the day. The NREM sleep, which represents the principal marker of process S during sleep, was also reduced after the night started and gradually increased as the day approached. Such EEG/EMG signal patterns are consistent with a normal sleep/wakefulness cycle of a nocturnal animal.

CA feeding significantly increased the EMG signals during the day as well as EEG signals (mostly the NREM waves) during the night, which together are consistent with the increased drowsiness during the day and restlessness during the evening as experienced by the cholemic patients with CLD (Figure 3*B and D−F*). These changes in EEG/EMG

Table 4. Blood Count and the Levels of PCT and CRP of Patients With CLD

	No cholemia (n = 29)	Cholemia (n = 31)	*P* value
WBC, × 10^9/*L*	4.45 (4.05–5.15)	4.0 (3.78–4.85)	.376
LYM, × 10^{12}/*L*	2.1 (1.6–2.8)	2.45 (1.83–2.88)	.374
MON, × 10^9/*L*	0.30 (2.15–0.44)	0.41 (0.26–0.56)	.227
NEU, × 10^9/*L*	3.7 (2.53–4.95)	4.0 (2.25–5.73)	.801
EOS, × 10^9/*L*	0.310 (0.16 –0.42)	0.310 (0.213 –0.400)	.838
BAS, × 10^9/*L*	0.030 (0.018–0.040)	0.035 (0.018–0.050)	.570
PCT, *ng/mL*	0.285 (0.24–0.62)	0.245 (0.168–0.35)	.152
CRP, *mg/L*	1.7 (0.65–2.53)	1.9 (0.65–2.53)	.378

BAS, Basophil; CLD, chronic liver disease; CRP, C-reactive protein; EOS, eosinophil; LYM, lymphocyte; MON, monocyte; NEU, neutrophil; PCT, procalcitonin; WBC, white blood cell.

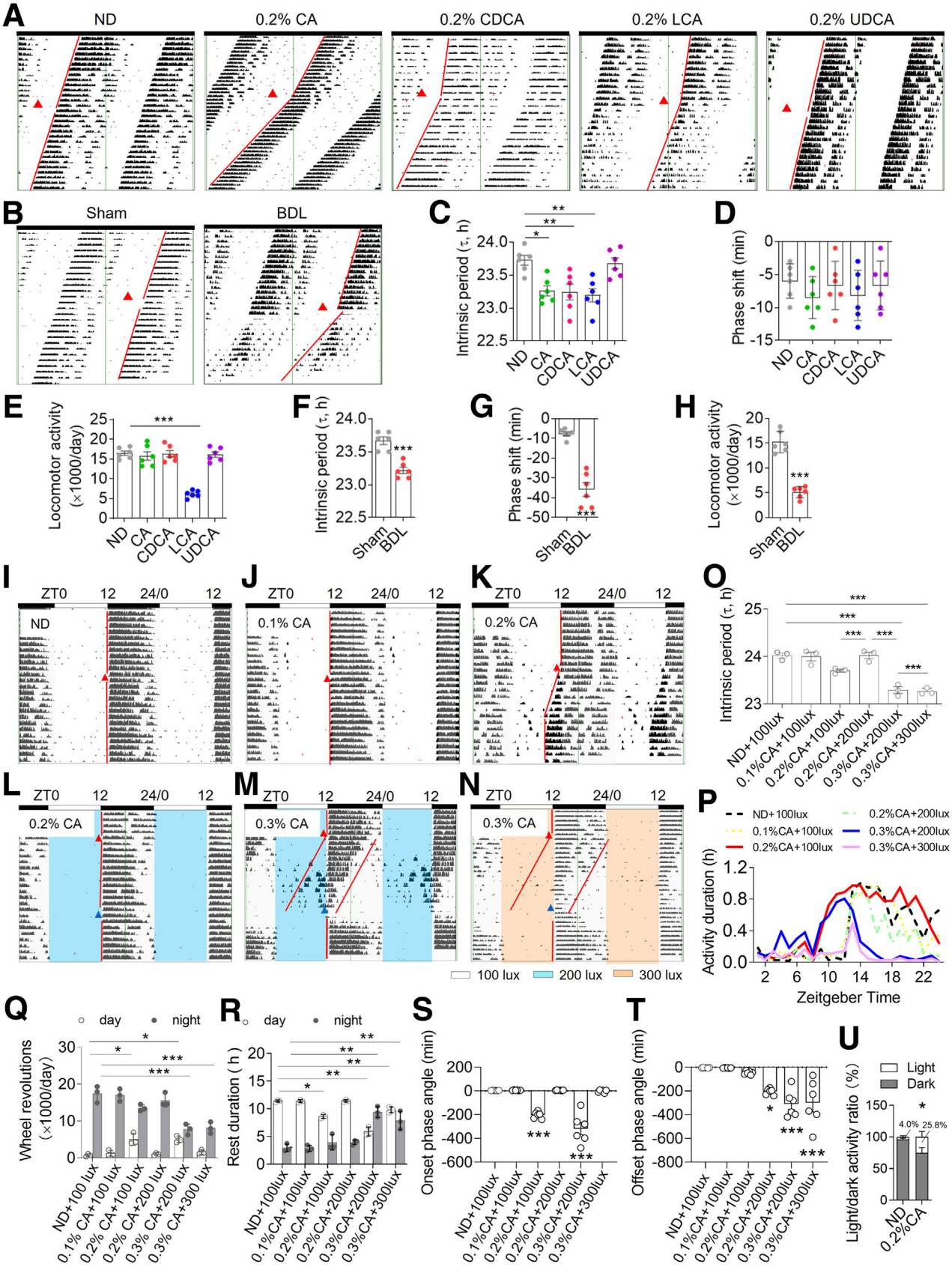
A
ND
0.2% CA
0.2% CDCA
0.2% LCA
0.2% UDCA
B
Sham
BDL
C
Intrinsic period (τ, h)
ND
CA
CDCA
LCA
UDCA
D
Phase shift (min)
E
Locomotor activity (×1000/day)
F
Intrinsic period (τ, h)
Sham
BDL
G
Phase shift (min)
H
Locomotor activity (×1000/day)
I
ZT0 12 24/0 12
ND
J
0.1% CA
K
0.2% CA
O
Intrinsic period (τ, h)
ND+100lux
0.1%CA+100lux
0.2%CA+100lux
0.2%CA+200lux
0.3%CA+200lux
0.3%CA+300lux
L
0.2% CA
M
0.3% CA
N
0.3% CA
100 lux
200 lux
300 lux
P
ND+100lux
0.1%CA+100lux
0.2%CA+100lux
0.2%CA+200lux
0.3%CA+200lux
0.3%CA+300lux
Activity duration (h)
Zeitgeber Time
Q
day
night
Wheel revolutions (×1000/day)
R
day
night
Rest duration (h)
S
Onset phase angle (min)
T
Offset phase angle (min)
U
Light
Dark
Light/dark activity ratio (%)
4.0%
25.8%
ND
0.2%CA

signals were almost completely reversed by CA withdrawal (Figure 3*C and D–F*). In particular, CA diet advanced the phase of wakefulness about 2 hours, which was reversed by CA withdrawal (Figure 3*D*). The REM sleep showed a similar phase change after CA feeding, which was partly restored by CA withdrawal, whereas the NREM sleep pressure became almost equally high in the night as in the day after CA feeding (ie, almost lost its original phase) (Figure 3*E and F*). These data demonstrate that the increased BA level affected sleep in a fashion similar to its effect on circadian rhythm. The impact of BA on the circadian process could build up a sleep deficiency with increased sleep pressure that affected NREM sleep via the homeostatic process.

BA Levels in the Cholemic Patients With CLD and Mouse Models

To better understand the role of BAs in CRSDs and better characterize the cholemic mouse models, we systemically examined the BA levels in the blood of the patients with CLD (Figure 4*A and B*) and in the blood and SCN tissues of the BDL and CA-fed mice (Figure 4*C–J*). Because the levels of total or individual BAs were almost identical in the non-cholemic CLDs, we grouped them as one data. The levels of TBA and individual BAs except 3-dihydrocaffeic acid (DHCA) were significantly higher in the cholemic patients with CLD than those in the non-cholemic patients with CLD (Figure 4*A and B*). The TBA levels in the PBC groups were higher than those of HB, hepatitis B cirrhosis (HBC), and NALC groups, consistent with a higher degree of cholestasis in PBC. CA, CDCA, and their glycine (not taurine) conjugated forms represented the abundant primary BAs, whereas deoxycholic acid (DCA), LCA, glycodeoxycholic acid (GDCA), and glycolithocholic acid (GLCA) were the predominant secondary BAs. Compared with the non-cholemic patients, CA, glycocholic acid (GCA), taurocholic acid (TCA), taurochenodeoxycholic acid (TCDCA), UDCA, glycoursodeoxycholic acid (GUDCA), and tauroursodeoxycholic acid (TUDCA) showed the greatest fold of increase in the cholemic patients with CLD. Notably, CA (as well as GCA and TCA) levels were increased in the cholemic patients with all 4 types of CLDs, suggesting CA as the most important BA in the cholemia of CLDs.

The serum TBA levels in the sham-operated and BDL mice were at comparable range as those in the noncholemic and cholemic patients with CLD (Figure 4*A–D*). In comparison, the serum TBA only rose to 10,000 ng/mL in the 0.2% CA-fed mice (Figure 4*B, D, H*). Thus, BDL, a widely used model for cholestasis, induced a comparable level of cholemia as in cholemic patients with CLD, whereas CA feeding provided a more moderate model sufficient to induce CRSD phenotypes. BDL induced 16 BA species to markedly rise in the serum, with TCA, α- tauro-muricholic acid (TMCA), TCDCA, and TUDCA being most dramatically increased (Figure 4*C and D*). BDL surgery also changed the TBA levels and BA profiles in the SCN similarly as in the systemic blood (Figure 4*E and F*), indicating that the permeability of the blood-brain barrier (BBB) was compromised. Leaky BBB has been reported in previous BDL models.[30,31]

In the CA-fed mice, the blood CA level was increased about 8-fold compared with the control mice (Figure 4*G and H*). The CA level remained largely unchanged in the SCN, which was not surprising as the BBB permeability likely remained intact in the CA-fed mice, given the moderate condition of 0.2% CA (Figure 4*I and J*). DCA was increased in both serum and SCN with ~8- and ~31-fold (Figure 4*G and I*), reflecting the massive conversion of CA to secondary BA by the gut bacteria. Similar rise of DCA was seen in the cholemic patients with CLD and the BDL mice, and has been reported in the CA-fed mice.[32] The secondary BAs are mainly eliminated in the colon through feces. However, a small amount of deconjugated secondary BAs can enter the circulation by passive diffusion and serve as potential signaling molecules. Hydrophobic BAs like DCA, which are potent agonists for Tgr5, also can diffuse across the BBB via passive diffusion and exert their action in the SCN.

BDL is known to induce inflammation,[33] which could affect circadian rhythm and complicate the interpretation of our findings. Therefore, we examined the hepatic and intestinal mRNA expression of cytokine *TNFα*, *IL-1β*, *IL-6*, and *IL-10* from the sham-operated and BDL mice as well as the ND or CA-fed mice (Figure 4*K–N*). The cytokine expression did not show significant difference in the liver and intestine in 14 days in the CA-fed mice, whereas they were markedly

Figure 2. (***See previous page***). **CRSD-like phenotypes in cholemic mice.** (*A*) Representative actograms of mice fed with ND or diet supplemented with 2% of CA, CDCA, LCA, and UDCA, running under DD conditions. *Red filled triangles* denote the beginning time of BA diet. N = 6. (*B*) Representative actograms of sham and BDL mice. Red filled triangles denote the beginning time of sham or BDL surgery. N = 3. (*C–E*) The intrinsic period, phase shift, and locomotor activities of the mice fed with ND and BAs. Mean ± SEM, 1-way ANOVA, Tukey's multiple comparisons test, $^{*}P < .05$; $^{**}P < .01$; $^{***}P < .001$ vs ND, N = 6. (*F–H*) The intrinsic period, phase shift, and locomotor activities of mice that underwent sham surgery and BDL. Mean ± SEM, unpaired *t*-test, $^{***}P < .001$ vs sham, N = 3. (*I–N*) Representative actograms of mice fed with different doses of CA under LD 12:12 environment with varying light intensities. N = 3. (*I*) ND + 100 lux. (*J*) 0.1% CA chow + 100 lux. (*K*) 0.2% CA chow + 100 lux. (*L*) 0.2% CA chow + 200 lux. (*M*) 0.3% CA chow + 200 lux. (*N*) 0.3% CA chow + 300 lux. The *gray areas* indicate darkness, *white areas* indicate exposure to 100 lux light, *blue areas* indicate exposure to 200 lux light, and *yellow areas* indicate exposure to 300 lux light. The *red filled triangles* indicate the beginning time of CA diet, and *blue filled triangles* denote the time to replace CA-containing diet with ND. N = 3. (*O–T*) The intrinsic period, activity duration, wheel revolution, rest duration, onset phase angle, and offset phase angle of the mice from panels *I–N*. Mean ± SEM, 1-way ANOVA for *O, S, and T*, 2-way ANOVA for *Q and R*, Tukey's multiple comparisons test, $^{*}P < .05$; $^{**}P < .01$; $^{***}P < .001$ vs ND + 100 lux, N = 3. (*U*) The light/dark activity ratio of the ND- and 0.2% CA-fed mice. Mean ± SEM, paired *t*-test, $^{*}P < .05$ vs ND, N = 3.

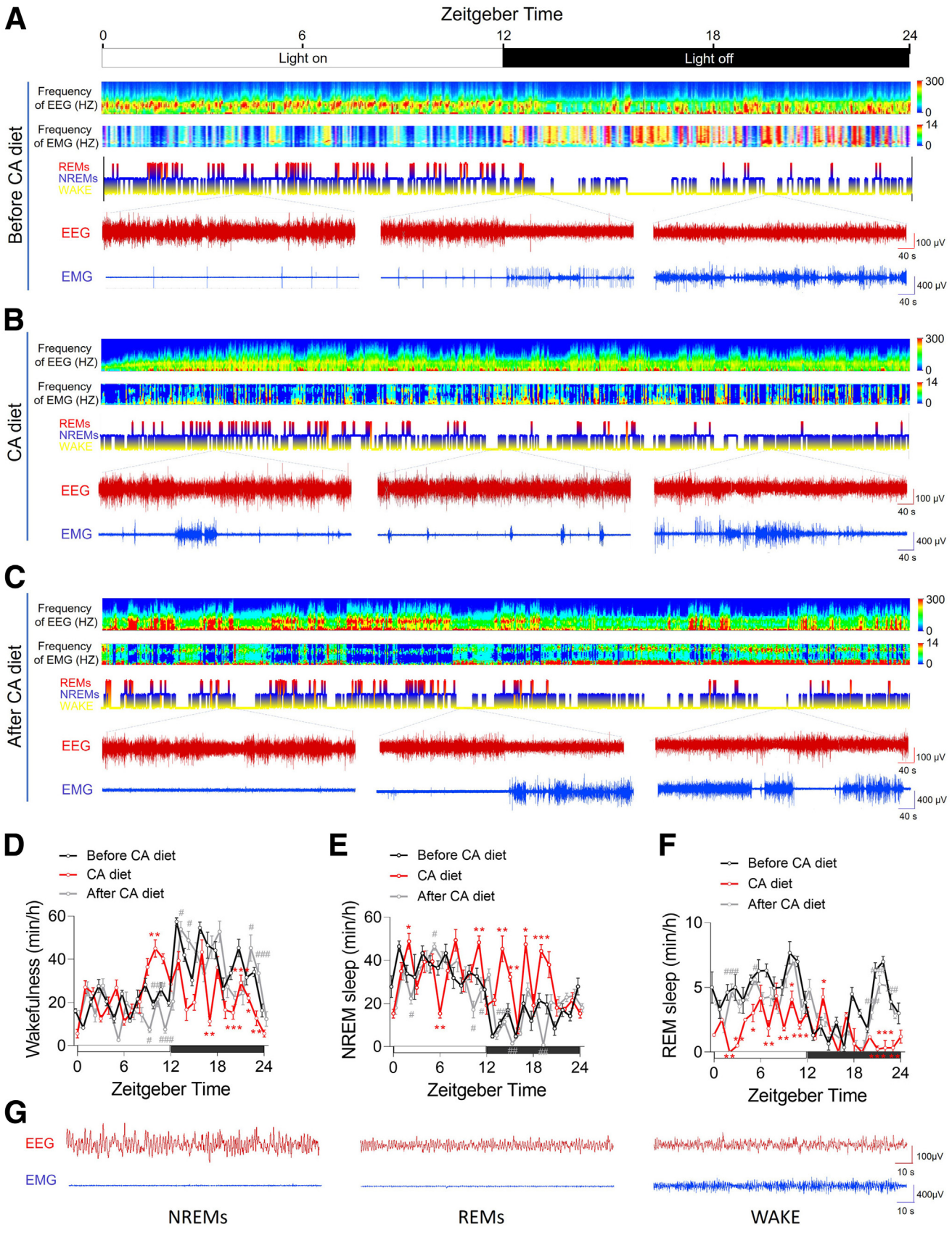
A
Zeitgeber Time
0
6
12
18
24
Light on
Light off
Before CA diet
Frequency of EEG (HZ)
Frequency of EMG (HZ)
REMs
NREMs
WAKE
EEG
EMG
300
0
14
0
100 μV
40 s
400 μV
40 s
B
CA diet
C
After CA diet
D
Before CA diet
CA diet
After CA diet
Wakefulness (min/h)
Zeitgeber Time
E
NREM sleep (min/h)
F
REM sleep (min/h)
G
EEG
EMG
100μV
10 s
400μV
10 s
NREMs
REMs
WAKE

increased 7 days after the BDL operation. The absence of systemic inflammation in the CA-fed mice, which was pronounced in the BDL model, confirmed feeding with 0.2% CA as an effective, nontoxic model, which was used in the following studies.

Increased BAs in the SCN-induced Changes in Circadian Rhythm

Next, we explored whether the rise of BA alone in the SCN was sufficient to alter circadian rhythm in mice by microinjection of CA into SCN. Three hours after 1 nmoL and 10 nmoL of CA was injected, the TBA level in the SCN was increased to 12 μM and 18 μM (Figure 5*A*), which completely or partly returned to the control level 10 hours after injection. Injection of 10 nmoL of CA did not induce any change in cytokine (*TNFα*, *IL-1β*, *IL-6*, and *IL-10*) expression (Figure 5*B*), indicating little inflammation in the injected SCN tissue. The locomotor activities showed that, compared with the mice injected with artificial cerebrospinal fluid (ACF), injection of 10 nmoL CA significantly shortened the circadian period in the mice running at DD (Figure 5*C and D*). Injection of 1 nmoL and 10 nmoL CA both induced a phase delay (Figure 5*E*). These data confirm that the increased BAs in the SCN accounts for the cholemia-induced shorter period, which is the fundamental mechanism underlying the early awakening and decreased sleep quality in mice under normal LD environment and the CRSD symptoms of patients with CLD.

CA Alters Circadian Oscillating Expression of Clock Genes and Increases Per2 Level in the SCN

Reverse transcription polymerase chain reaction (RT-PCR) analysis showed that the mRNA oscillation peaks of *Clock*, *Bmal1*, *Per1,* and *Per2* genes in the SCN of the mice were shifted forward about 4 hours, with a shortened period after the mice were fed with CA diet for 1 week, although their expression levels were similar compared with the ND-fed mice (Figure 5*F*). Consistent with the transcript levels, the protein levels of Clock, Bmal1, Per1, and Cry1 were largely unchanged in the SCN of the mice fed with increasing amount of CA (Figure 5*G and H*). However, Per2 level was increased in a dose-dependent manner in the SCN of CA-fed mice. As examined by immunoblotting, the specificity of the commercial antibodies against the clock proteins used in this study was validated by overexpression using constructs encoding mouse *Clock*, *Bmal1*, *Per1*, *Per2,* and *Cry1* and RNA interference (RNAi) with small interfering RNAs (siRNAs) targeting the clock genes in mouse NIH3T3 cells (Figure 5*I and J*). We also analyzed the expression of Clock, Bmal1, Per1, Per2, and Cry1 in the SCN at CT 10 and CT 22 from the CA-fed mice by immunofluorescence, which showed similar oscillating expression pattern as detected by RT-qPCR (Figure 5*K and L*). Importantly, consistent with the immunoblotting data, only the expression of Per2, not other clock proteins, was induced by CA treatment.

CA Alters the Level, Phosphorylation, and Nucleo-cytoplasmic Distribution of Per2

To explore the role of Per2 in rhythm disturbance in cholemic mice, we examined the expression and subcellular distribution of Per2 in SCN neurons. The immunofluorescent staining showed that CA increased the level of Per2 and especially in the cytoplasm of SCN neurons (Figure 6*A and B*). We verified Per2's distribution by separation of nuclear and cytoplasmic proteins. Compared with the control mice, Per2 was reduced in the nuclear fraction but increased in the cytosolic fraction of the SCN of the CA-fed mice (Figure 6*C and D*). The CA-induced nucleocytoplasmic redistribution was confirmed in the NIH/3T3 cells. After applying the serum shock, the Per2 level showed a circadian rhythmic oscillation in NIH/3T3 cells: reaching a trough at approximately 12 hours and a peak at 24 hours (Figure 6*E*). Immunofluorescence showed that Per2 in the control cells was mainly in the cytoplasm 12 hours after serum shock and localized to the nucleus 24 hours after serum shock (Figure 6*F, G, and H*), whereas CA treatment markedly increased the cytoplasmic/nuclear ratio of Per2 at 24 hours after serum shock (Figure 6*F, G, and H*). Immunoblotting with a phosphor-specific antibody revealed that phosphorylation of Per2 at Ser478 was increased in the SCN after the mice were treated with 0.1% or 0.2% CA but not with 0.3% CA (Figure 6*I and J*). Locomotor activity analysis of *Per2*$^{-/-}$ mice showed that their free-running period was shorter than that of the wild-type (WT) mice running at DD (Figure 6*K and L*). Feeding with 0.2% CA could not further shorten the free-running period of *Per2*$^{-/-}$ mice (Figure 6*K and L*), confirming that Per2 was the target mediating the CA's rhythm-altering effects.

Tgr5 Mediates the CA-induced Changes in Per2 and Circadian Period Shortening

Next, we characterized the signaling pathway upstream of Per2 in the CA-fed cholemic mouse model. BAs are known to interact with both intracellular nuclear receptors, mainly

Figure 3. (***See previous page***). **Sleep-wake rhythm disturbance in cholemic mice.** (*A–C*) Representative EEG, EMG power spectra, and hypnogram during a 24-hour period and representative 400s-EEG and EEG actographs at day, day-night alternation, and night under the baseline (*A*), CA diet (*B*), and CA diet withdrawal (*C*) condition. N = 3. (*D–F*) Wakefulness (*D*), NREM sleep (*E*), and REM sleep (*F*) duration during the 24-hour period in panels *A*−*C*. Mean ± SEM, 2-way ANOVA, Tukey's multiple comparisons test, $^{*}P < .05$; $^{**}P < .01$; $^{***}P < .001$ vs baseline, $^{\#}P < .05$; $^{\#\#}P < .01$; $^{\#\#\#}P < .001$ vs CA diet, N = 3. (*G*) Representative EEG and EMG for NREMS, REMS, and WAKE of mice. The *open and closed bars* indicate the light and dark periods, respectively.

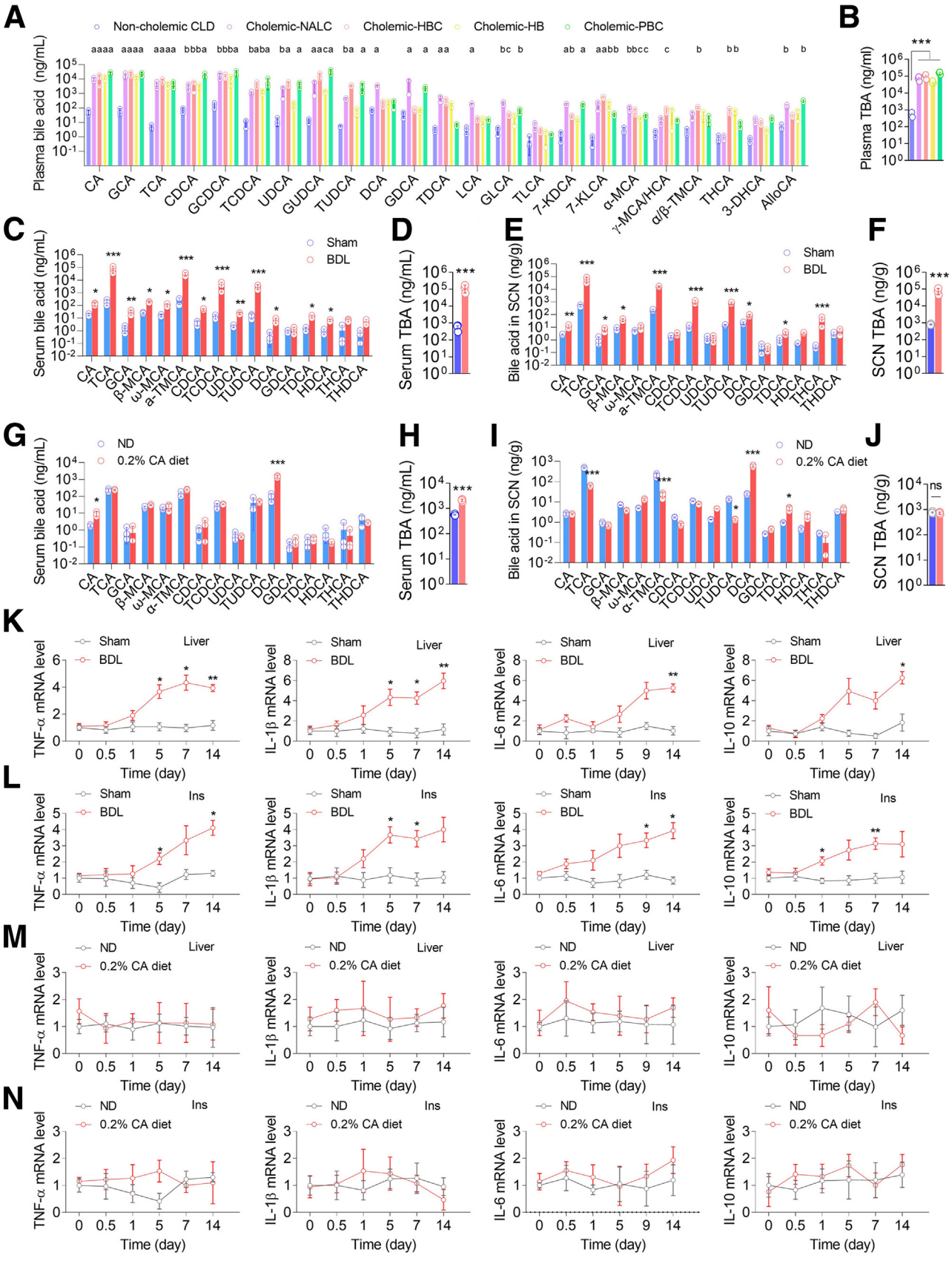
A
Non-cholemic CLD
Cholemic-NALC
Cholemic-HBC
Cholemic-HB
Cholemic-PBC
Plasma bile acid (ng/mL)
CA GCA TCA CDCA GCDCA TCDCA UDCA GUDCA TUDCA DCA GDCA TDCA LCA GLCA TLCA 7-KDCA 7-KLCA α-MCA γ-MCA/HCA d/β-TMCA THCA 3-DHCA AlloCA
B
Plasma TBA (ng/ml)
C
Serum bile acid (ng/mL)
Sham
BDL
CA TCA GCA β-MCA ω-MCA α-TMCA CDCA TCDCA UDCA TUDCA DCA GDCA TDCA HDCA THCA THDCA
D
Serum TBA (ng/mL)
E
Bile acid in SCN (ng/g)
F
SCN TBA (ng/g)
G
Serum bile acid (ng/mL)
ND
0.2% CA diet
H
Serum TBA (ng/mL)
I
Bile acid in SCN (ng/g)
J
SCN TBA (ng/g)
ns
K
TNF-α mRNA level
IL-1β mRNA level
IL-6 mRNA level
IL-10 mRNA level
Sham
BDL
Liver
Time (day)
L
Ins
M
ND
0.2% CA diet
N

the farnesoid X receptor (FXR), preganane X receptor (PXR), and the vitamin D receptor (VDR), and transmembrane G protein-coupled receptors, mainly the Takeda G-protein-coupled receptor 5 (TGR5). RT-PCR analysis show that the mRNA levels of *Pxr* and *Vdr* were undetectable in the cerebellum, brainstem, hypothalamus, and cortex of mice, whereas the mRNA expression of *Tgr5* and *Fxr* varied in various brain regions (Figure 7*A*). *Tgr5* was expressed at much higher levels than *Fxr* in the hypothalamus and cortex. The Tgr5 protein level was also higher in the hypothalamus and cortex than in other brain regions (Figure 7*B*). Importantly, the *Tgr5* mRNA and protein in mouse SCN exhibited a 24-hour circadian rhythm with the highest level at ZT10 and the lowest level at ZT22−ZT2 (Figure 7*C and D*). Immunohistochemistry confirmed that Tgr5 was expressed across the entire SCN, with a concentration in the ventral retinorecipient core at ZT10 and an oscillatory rhythm in the SCN of the control mice (Figure 7*E*). When 1 nmoL or 10 nmoL CA was injected into the SCN at CT15, *Tgr5* mRNA expression was significantly increased 3 hours after injection (Figure 7*F*), and the induced Tgr5 protein was mainly localized to the ventral core (Figure 7*G*). The levels of *Tgr5* mRNA and protein remained at a high level even 10 hours after injection of 10 nmoL CA. We speculated that Tgr5 mediated the effect of CA on Per2.

To that end, we first injected oleanolic acid (OA), a Tgr5 agonist, into the mouse SCN at ZT15 and examined the mRNA and protein level of *Tgr5* in the SCN together with the wheel running activity 2 hours after injection (ZT17). Injection of 10 nmoL OA induced evident elevation of *Tgr5* mRNA (Figure 7*H*) but no change in cytokine (*TNFα*, *IL-1β*, *IL-6,* and *IL-10*) expression (Figure 7*I*), indicating no inflammation in the injected SCN tissue. Injection of 10 nmoL of OA shortened the circadian period of the mice running at DD, as compared with the ACF-injected mice (Figure 7*J and K*). In addition, OA injection of 1 nmoL and 10 nmoL both induced a significant phase shift (Figure 7*L*). We further proved the role of Tgr5 in CA-induced rhythmic changes using RNAi. The injection of adeno-associated virus (AAV) against *Tgr5* reduced Tgr5 protein level (Figure 7*M*) and reversed the CA-induced period shortening, as compared with the mice injected with the scrambled AAV (Figure 7*N and O*). These results demonstrate that Tgr5 is the key BA receptor mediating the CA-induced rhythmic changes.

Erk-CK1ε Pathway Mediates the CA-induced Changes Downstream of Tgr5

Mechanistically, TGR5 activates a number of downstream signaling targets, including the cAMP-PKA, ERK, AKT, and transient receptor potential ankyrin 1 (TRPA1).[34] We examined the expression of these downstream targets in the SCN from the mice fed with increasing amount of CA and found that the expression level of extracellular signal-regulated kinase (Erk) and phosphorylated Erk (p-Erk) were increased similarly as Tgr5 after CA feeding, whereas the expressions of Pka, Akt, and Trpa1 remained unchanged (Figure 8*A and B*). In addition to Erk, the protein level of CK1ε but not CK1δ was also increased after CA feeding as shown by both immunoblotting (Figure 8*A and B*) and immunofluorescence (Figure 8*C and D*).

We then functionally verified the role of Erk by injection of 0.2 μmoL of temuterkib, an Erk1/2 inhibitor, into the SCN of the mice at CT6 running at DD. We then fed the mice with 2% CA at CT12 ,and their circadian locomotor rhythms were monitored for 10 days. Like Tgr5 RNAi, temuterkib effectively reversed the CA-induced shortening of circadian period (Figure 8*E and F*). Similar to CA feeding, injection of 10 nmol CA into the mouse SCN increased the levels of Tgr5, p-Erk, and CK1ε (Figure 8*G and H*). These effects were reversed by the co-injection of SBI-115, a Tgr5 antagonist, as well as by temuterkib, but were reinforced by the co-injection of ML-184, an Erk agonist (Figure 8*G and H*). Together, these results demonstrate that Erk and CK1ε partake in the signaling pathway downstream of Tgr5, mediating the CA-induced CRSDs in the cholemic mice.

CA Blunts the Light-induced Phase Shift via the Tgr5-Per2 Pathway in the GRP-expressing Neurons

SCN contains several types of neurons in its ventral and dorsal region. The gastrin releasing peptide (GRP)-, vasoactive intestinal peptide (VIP)-, and arginine vasopressin (AVP)-expressing neurons have previously suggested to closely integrate into SCN's neural network.[35] Double-labeled immunofluorescent staining showed a colocalization of TGR5 in the GRP-expressing neurons, whereas little TGR5 was detected in the AVP- and VIP-expressing neurons (Figure 9*A*), suggesting that TGR5 and BA signaling act via the GRP neurons. The GRP-expressing neurons are known to

Figure 4. (***See previous page***). **BA levels in the cholemic patients with CLD and cholemia mouse models.** The levels of serum individual (*A*) and total (*B*) BAs of noncholemic and cholemic patients with CLD. Mean ± SEM, 2-way ANOVA, Tukey's multiple comparisons test; a, b, and c, respectively, indicate $P < .05$, $P < .01$, and $P < .001$ vs non-cholemic CLD, ***$P < .001$ vs non-cholemic CLD, N = 3. The levels of serum individual (*C*) and total (*D*) BAs in sham-operated and BDL mice. Mean ± SEM, 2-way ANOVA, Tukey's multiple comparisons test, *$P < .05$; **$P < .01$; ***$P < .001$ vs sham, N = 3. The levels of individual (*E*) and total (*F*) BAs in the SCN of the sham-operated and BDL mice. Mean ± SEM, 2-way ANOVA, Tukey's multiple comparisons test, *$P < .05$; **$P < .01$; ***$P < .001$ vs sham, N = 3. The levels of serum individual (*G*) and total (*H*) BAs in mice fed with ND or chow supplemented with 0.2% CA. Mean ± SEM, unpaired 2-tailed *t*-test, ***$P < .001$ vs ND, N = 3. The levels of individual (*I*) and total (*J*) BAs in the SCN of the mice fed with ND or chow supplemented with 0.2% CA. Mean ± SEM, 2-way ANOVA, Tukey's multiple comparisons test, **$P < .01$ vs ND, N = 3. The liver (*K*) and intestinal (*L*) levels of *TNFα*, *IL-1β*, *IL-6,* and *IL-10* mRNA from the sham-operated and BDL mice. Mean ± SEM, 2-way ANOVA, Tukey's multiple comparisons test, *$P < .05$; **$P < .01$ vs sham, N = 3. The liver (*M*) and intestinal (*N*) levels of *TNFα*, *IL-1β*, *IL-6,* and *IL-10* mRNA from the ND-fed and CA-fed mice. Mean ± SEM, 2-way ANOVA, Tukey's multiple comparisons test, N = 3.

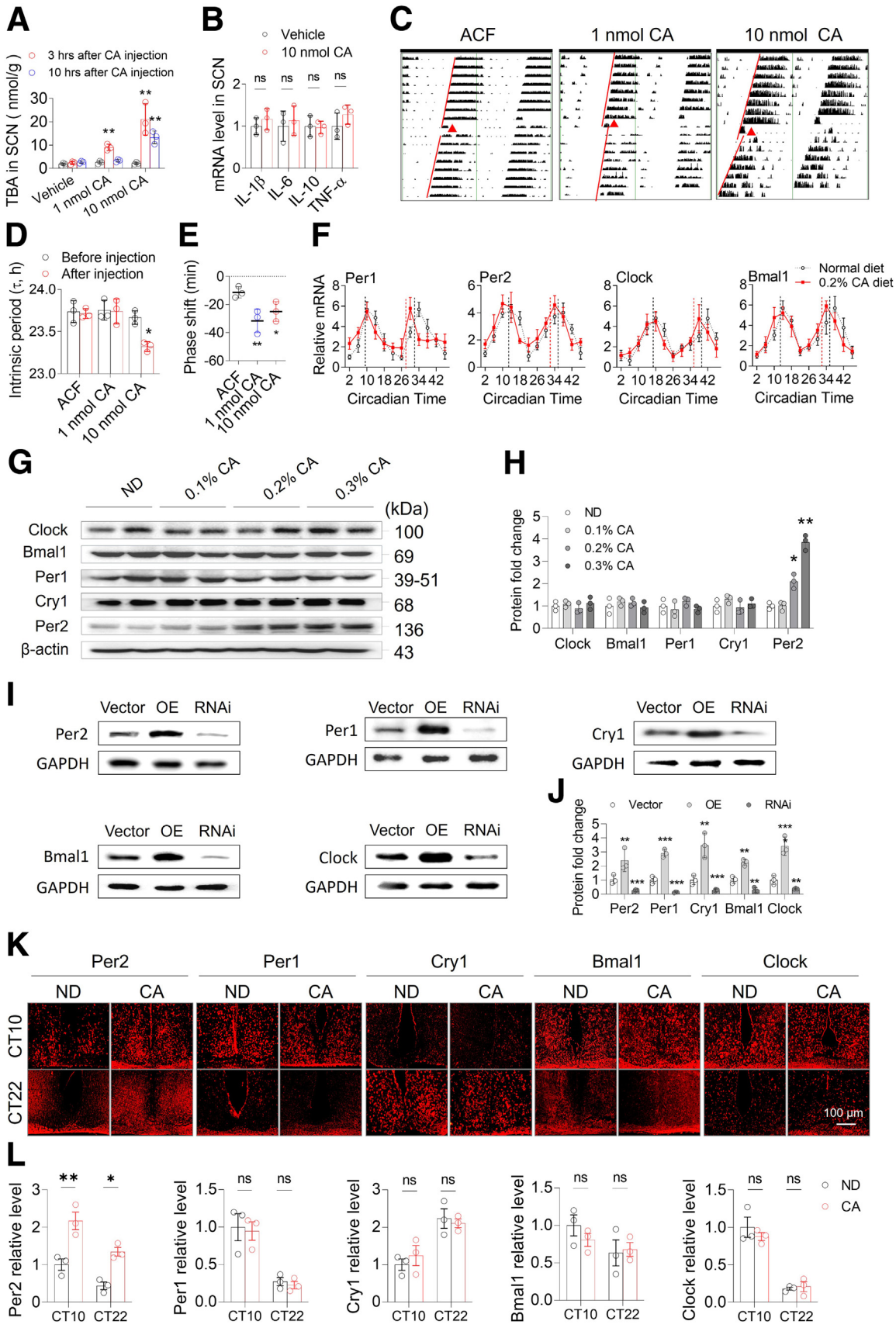
A
3 hrs after CA injection
10 hrs after CA injection
TBA in SCN (nmol/g)
Vehicle
1 nmol CA
10 nmol CA
B
Vehicle
10 nmol CA
mRNA level in SCN
IL-1β
IL-6
IL-10
TNF-α
C
ACF
1 nmol CA
10 nmol CA
D
Before injection
After injection
Intrinsic period (τ, h)
E
Phase shift (min)
F
Per1
Per2
Clock
Bmal1
Relative mRNA
Circadian Time
Normal diet
0.2% CA diet
G
ND
0.1% CA
0.2% CA
0.3% CA
(kDa)
Clock
Bmal1
Per1
Cry1
Per2
β-actin
100
69
39-51
68
136
43
H
Protein fold change
I
Vector OE RNAi
Per2
Per1
Cry1
Bmal1
Clock
GAPDH
J
K
CT10
CT22
100 μm
L
Per2 relative level
Per1 relative level
Cry1 relative level
Bmal1 relative level
Clock relative level

localize to the SCN ventral retinorecipient zone, from which they communicate the photic resetting signals received from retina to other neurons within the SCN network. Injection of GRP into the SCN region can induce phase shift and activation of *Per* gene.[36,37] Therefore, we speculated that activation of TGR5 by BAs may influence the synthesis or secretion of GRP, which in turn changes the light-induced phase shift responses. To verify this speculation, we monitored the light-induced phase shift at ZT15 or ZT22 in C56BL/6J mice and found that injection of CA or OA into the SCN at ZT6 partially abolished the light-induced phase shift effects (Figure 9*B*–*E*). Consistent with its critical role in phase regulation, CA or OA also abolished the light pulse-induced elevation of *Per2* mRNA (Figure 9*F*) but not *Per1* mRNA (Figure 9*G*). Immunohistochemistry further shows that the levels of TGR5 and GRP protein were low in the SCN of ACF-injected mice but were increased soon after light pulse given at ZT15 (Figure 9*H, I, and J*). Injection of CA or OA into the SCN partly blunted the light-induced increase in TGR5 and GRP (Figure 9*H, I, and J*). Together, these results confirmed that CA blunts the light entrainment via the Tgr5-Per2 pathway in the Grp-expressing neurons of the SCN.

Drugs Lowering BA Level and Enhancing Per2 Stability Reverse CRSD in Cholemic Mice

As mentioned above, cholemia induced the CRSDs in mice by affecting the nucleocytoplasmic distribution of Per2 in the SCN. We next tested the possibility whether decreasing circulatory BAs level by cholestyramine (CHO), a BA sequestrant that binds to BAs in the intestine and blocks BA absorption, could rescue the cholemic mice from the CRSD-like phenotypes. In these experiments, we also tested the effects of PF-670462, a selective CK1ε/δ inhibitor. We first monitored the rest-activity rhythms of 0.2% CA-fed mice for at least 2 weeks running at DD, then fed with a diet further supplemented with 6% CHO (*w*/*w*) or subcutaneously injected PF-670462 (50 mg/kg) at CT6 every day for 2 weeks (Figure 10*A and B*). Treatment with CHO and PF-670462 both extended the voluntary rest-activity period of CA-fed mice close to the normal free-running period of the control mice (Figure 10*A*–*D*). In addition, the serum and SCN TBA levels and the oscillating expression of *Per2* in the CA-fed mice were restored to those of the control mice 1 week after CHO or PF-670462 treatment (Figure 10*E*–*H*). These results showed that CHO and PF-670462 reversed the CRSDs in cholemic mice running under DD through Per2. We also explored the therapeutic effects of CHO and PF-670462 on the CRSDs in the CA-fed mice running under the regular LD: 12:12 environment. The wheel-revolutions and the day/night activity ratio of the CA-fed mice treated with CHO and PF-670462 were restored to those of the ND-fed mice (Figure 10*I*–*L*). In addition, PF-670462 treatment also reduced the levels of CK1ε and CK1δ in the SCN (Figure 10*M*), as well as reversing the nucleocytoplasmic distribution of Per2 (Figure 10*N*). Thus BA sequestrant and CK1ε/δ inhibitor also reversed the irregular rhythms in cholemic mice running under regular LD condition through Per2.

Discussion

In this study, we first identified elevated level of BAs as a major risk factor for CRSDs in patients with CLD. Then we demonstrated that the increase of BAs in the blood and SCN is sufficient to induce shorter circadian period and phase shift, which are fundamental to the CRSD-like phenotypes in the cholemic patients with CLD, using 2 cholemic mouse models. Next, we showed that BAs activate Tgr5 in the SCN, which in turn phosphorylates Erk, CK1ε, and eventually Per2 (Graphical Abstract). Per2 phosphorylation at Ser478 mitigates its nuclear import with a net effect of fewer Per2/Cry complex in the nucleus, which would release the Clock/Bmal1 complex from inhibition by Per2/Cry and allow *Per*/*Cry* transcription to resume. These would result in an expedited circadian period and advanced phase (Graphical Abstract).

Metabolites, including BAs, can gain access to the brain under some pathophysiological conditions, partly as a result of the leaky BBB or high hydrophobicity (Graphical Abstract). Two studies suggested that BAs played a role in HE and ataxia once they crossed the BBB.[38,39] Other proposed mechanisms for the SDs in CLDs include impaired melatonin metabolism, impaired thermoregulation, and increased ammonia level, all of which result from impaired liver function. Because CLDs are complex and other pathogenic factors could precede cholestasis in their etiology, BAs likely

Figure 5. (***See previous page***). **Circadian rhythmic changes induced by CA injected into the SCN and circadian oscillation of the clock genes in the SCN.** (*A*) TBA levels in SCN at 0, 3, and 10 hours after injection of 1 nmoL CA or 10 nmoL CA into SCN. Mean ± SEM, 2-way ANOVA, Tukey's multiple comparisons test, $^{**}P < .01$, vs ACF-injected mice, N = 3. (*B*) The mRNA levels of TNFα, IL-1β, IL-6, and IL-10 in the SCN from the mice injected with vehicle ACF or 10 nmoL CA. Mean ± SEM, 2-way ANOVA, Tukey's multiple comparisons test, N = 3. (*C*) Representative wheel-running actograms of mice after injection of ACF, 1 nmoL CA, and 10 nmoL CA to SCN at CT15 under DD condition. *Red triangles* indicate the time of SCN injection. Intrinsic period (*D*) and phase shift (*E*) of the mice injected with CA or ACF into SCN. Mean ± SEM, 2-way ANOVA for D and 1-way ANOVA for E, Tukey's multiple comparisons test, $^{*}P < .05$; $^{**}P < .01$, vs ACF, N = 3. (*F*) Relative mRNA levels of *Per1*, *Per2*, *Clock,* and *Bmal1* in the SCN of the mice fed with ND or diet containing 0.2% CA for 1 week. Two circadian cycles were shown. N = 3. Note that CA feeding shortened the free-running period. Representative immunoblots (*G*) and quantitation (*H*) of the clock proteins Clock, Bmal1, Per1, Cry1, and Per2 in the SCN after mice were fed with increasing amount of CA (0.1%, 0.2%, and 0.3%) for 1 week. Mean ± SEM, 1-way ANOVA, Tukey's multiple comparisons test, $^{*}P < .05$; $^{**}P < .01$ vs ND, N = 3. Representative immunoblots (*I*) and quantitation (*J*) of Clock, Bmal1, Per1, Cry1, and Per2 in the NIH3T3 cells overexpressing (OE) the mouse clock genes or NIH3T3 cells with the mouse clock genes silenced by RNAi. Mean ± SEM, 1-way ANOVA, Tukey's multiple comparisons test, $^{**}P < .01$; $^{***}P < .001$ vs vector, N = 3. Immunofluorescent staining (*K*) and quantitation (*L*) of Per2, Per1, Cry1, Bmal1, and Clock in the SCN tissues harvested at CT10 and CT22 from the mice fed with ND or 0.2% CA. Mean ± SEM, 2-way ANOVA, Tukey's multiple comparisons test, $^{*}P < .05$; $^{**}P < .01$ vs ND, N = 3.

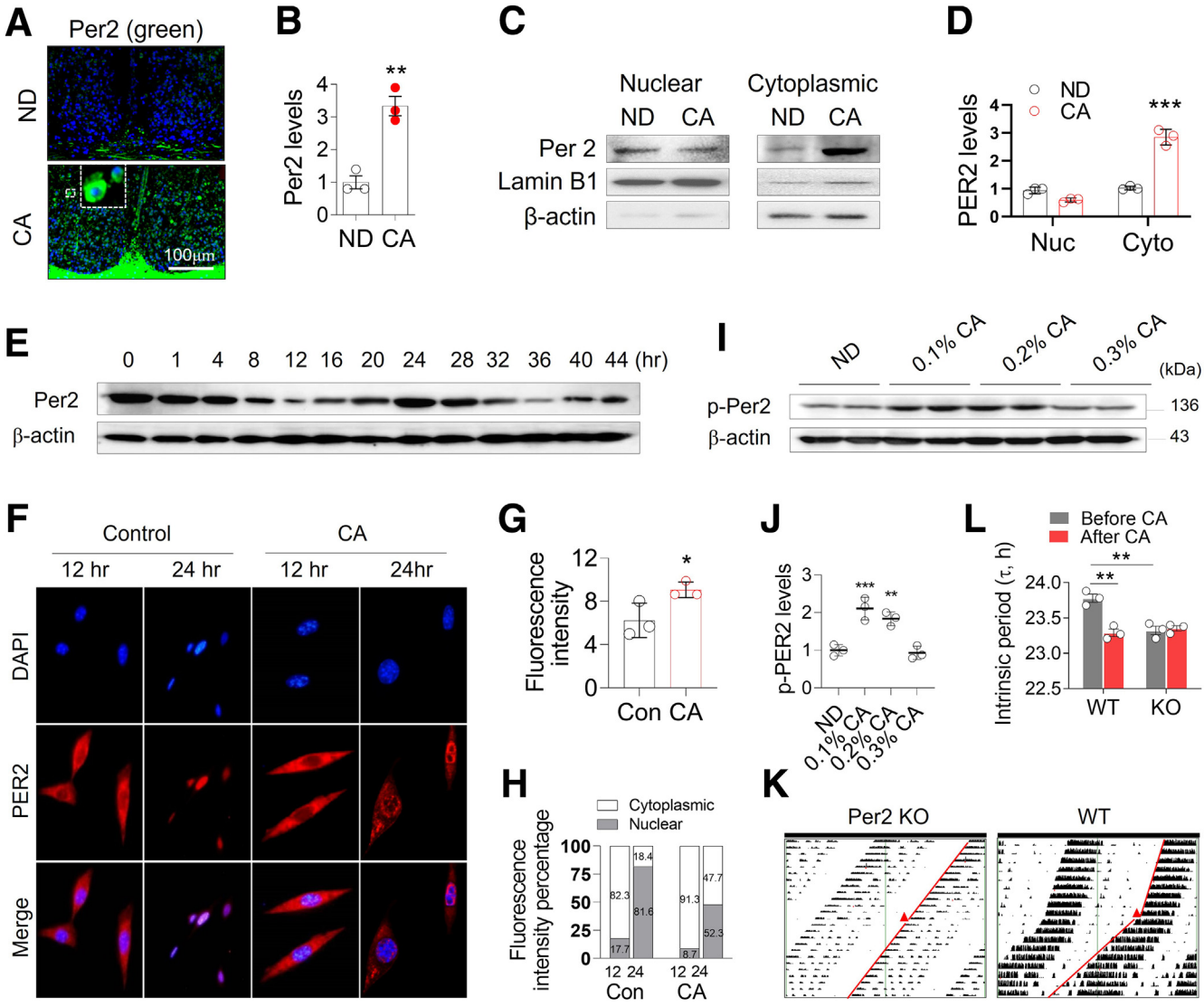

Figure 6. Per2 plays a crucial role in CA-induced period shortening. Immunofluorescent staining (*A*) and semi-quantification (*B*) of Per2 in the SCN of ND-fed or CA-fed mice under DD condition. *Green*, Per2. *Blue*, DAPI (nuclei). Mean ± SEM, unpaired 2-tailed *t*-test, $^{**}P < .01$ vs ND, N = 3. Immunoblots (*C*) and quantitation (*D*) of the nuclear and cytoplasmic expression of Per2 from the SCN after mice were fed with ND or CA for 1 week. Lamin B1 and β-actin serve as markers for the nucleus and cytoplasm, respectively. Mean ± SEM, paired 2-tailed *t*-test, $^{***}P < .001$ vs ND, N = 3. (*E*) Per2 protein rhythmic expression in NIH3T3 cells within 44 hours after serum shock. Immunofluorescent staining (*F*) and quantitation (*G and H*) of Per2 in NIH3T3 cells 12 hours and 24 hours after serum shock. Note that Per2 shuttles between nucleus and cytoplasm under normal condition, whereas CA induced an appreciable increase of total Per2 with significant decrease of nuclear/cytoplasmic ratio. Mean ± SEM, unpaired 2-tailed *t*-test, $^{*}P < .05$ vs ND, N = 3. Immunoblots (*I*) and quantitation (*J*) of pPer2 (Per2 phsphorylated at Ser478) in the SCN after mice were fed with increasing amount of CA (0.1%, 0.2%, and 0.3%) for 1 week. Mean ± SEM, 1-way ANOVA, Tukey's multiple comparisons test, $^{**}P < .01$; $^{***}P < .001$ vs ND, N = 3. (*K*) Representative wheel-running actograms and intrinsic periods (*L*) of WT and Per2 KO mice under DD condition before and after feeding with 0.2% CA. *Red filled triangles* denote the beginning time of 0.2% CA diet. Mean ± SEM, paired 2-tailed *t*-test, $^{**}P < .01$ vs WT or before receiving CA diet, N = 3.

represent only one potential mechanism in the SDs of CLDs. This is relevant, as the patients with CLD could manifest other SD types besides CRSDs, and most of our mechanisms were investigated using the BA feeding model not the BDL model, in which inflammation and other pathologies could disrupt sleep too.

In mammalians, the circadian system has a 2-hour plasticity around its internal period.[21] The circadian period of CA-fed mice was shortened to about 23.2 hours, which theoretically should be able to synchronize to the 24-hour external LD cycle. However, the light-induced phase shift was both blunted in the CA-fed mice. The light signal is

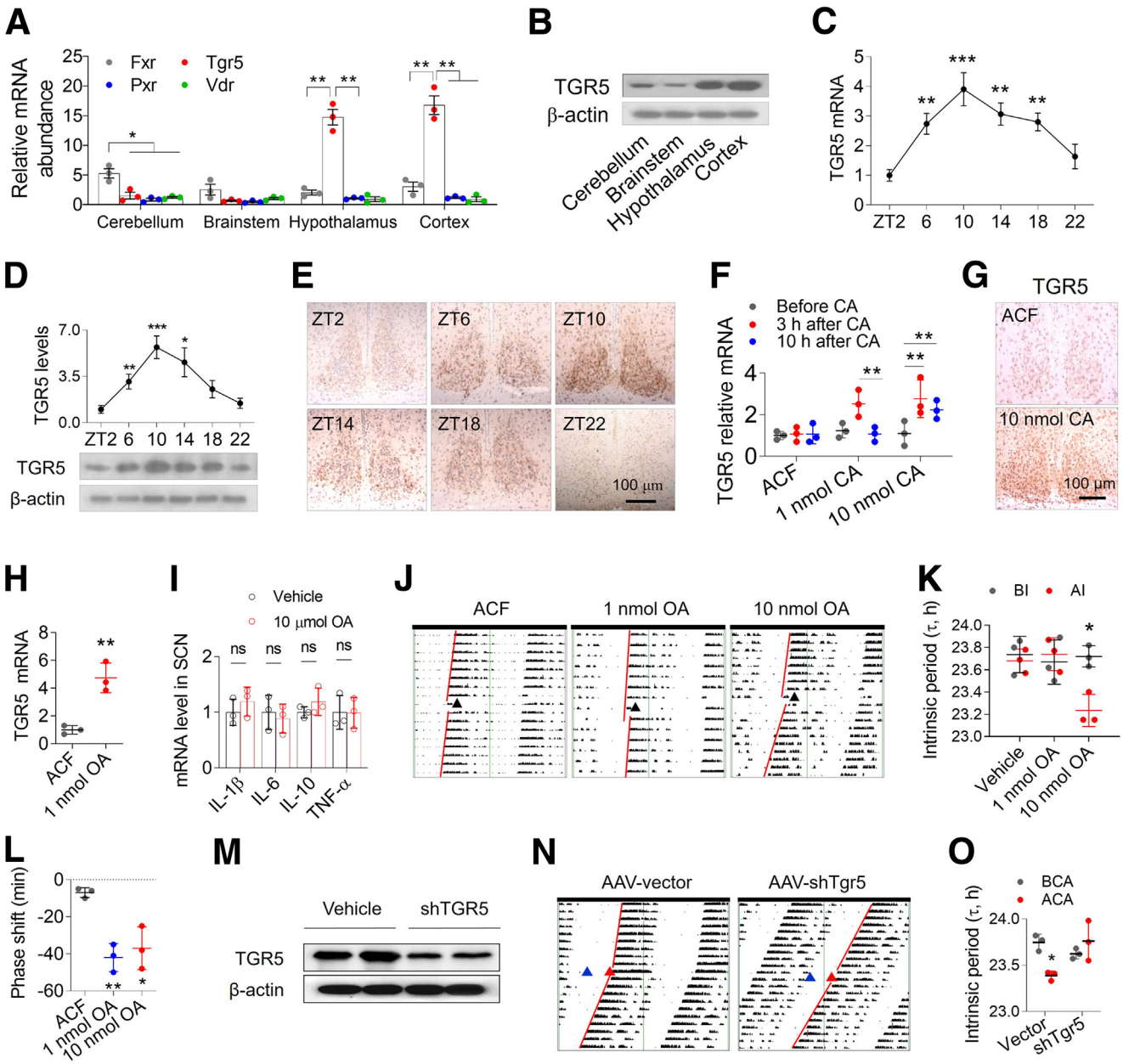

Figure 7. Tgr5 is expressed in SCN and mediates the CA-induced period shortening. (*A*) Relative mRNA levels of *Fxr*, *Tgr5*, *Pxr,* and *Vdr* in the cerebellum, brainstem, hypothalamus, and cortex of mice. Mean ± SEM, 2-way ANOVA, Tukey's multiple comparisons test, **P* < .05; ***P* < .01, vs other brain regions, N = 3. (*B*) Immunoblots of TGR5 in the cerebellum, brainstem, hypothalamus, and cortex. N = 3. (*C*) Oscillating expression of *Tgr5* mRNA in the SCN. Mean ± SEM, 1-way ANOVA, Tukey's multiple comparisons test, **P* < .05; ***P* < .01 vs ZT2, N = 3. (*D*) Circadian oscillations of TGR5 protein in the SCN with a representative immunoblot shown underneath. Mean ± SEM, 1-way ANOVA, Tukey's multiple comparisons test, **P* < .05; ***P* < .01 vs ZT2, N = 3. (*E*) Immunohistochemical staining showing the circadian oscillation of TGR5 in mouse SCN. N = 3. (*F*) *Tgr5* mRNA levels at 3 hours and 10 hours after injection of 1 nmoL CA and 10 nmoL CA into the SCN at CT15. Mean ± SEM, 2-way ANOVA, Tukey's multiple comparisons test, ***P* < .01 vs before CA or 3 hours after CA, N = 3. (*G*) Immunohistochemical staining of TGR5 at 3 hours after injection of 10 nmoL CA into the SCN of mice at CT15. (*H*) *Tgr5* mRNA levels in the SCN after 1 nmoL OA injection at CT15. Mean ± SEM, unpaired 2-tailed *t*-test, ***P* < .01 vs ACF, N = 3. (*I*) mRNA levels of *TNFα*, *IL-1β*, *IL-6,* and *IL-10* in the SCN after injection of 10 nmoL OA at CT15. Mean ± SEM, 2-way ANOVA, Tukey's multiple comparisons test, N = 3. Representative wheel-running actograms (*J*) of the mice with 10 nmoL OA or ACF injected into SCN with the intrinsic period (*K*) and phase shift (*L*) shown. *Black triangles* indicate the SCN injection time of OA or ACF. Mean ± SEM, 2-way ANOVA, Tukey's multiple comparisons test, **P* < .05 vs before injection, **P* < .05; ***P* < .01 vs ACF, N = 3. (*M*) Immunoblots of TGR5 in the SCN of the mice injected with AAV9-shTgr5 virus or control shRNA. N = 3. Actograms (*N*) of the mice injected with AAV9-shTgr5 virus or control shRNA and their intrinsic periods (*O*). *Blue triangle* indicates the injection time of AAV-shTGR5 or ACF (at CT6), and *red triangles* denote the beginning time of 0.2% CA diet. BCA: before CA diet, ACA: after CA diet. Mean ± SEM, paired 2-tailed *t*-test, **P* < .05 vs BCA, N = 3.

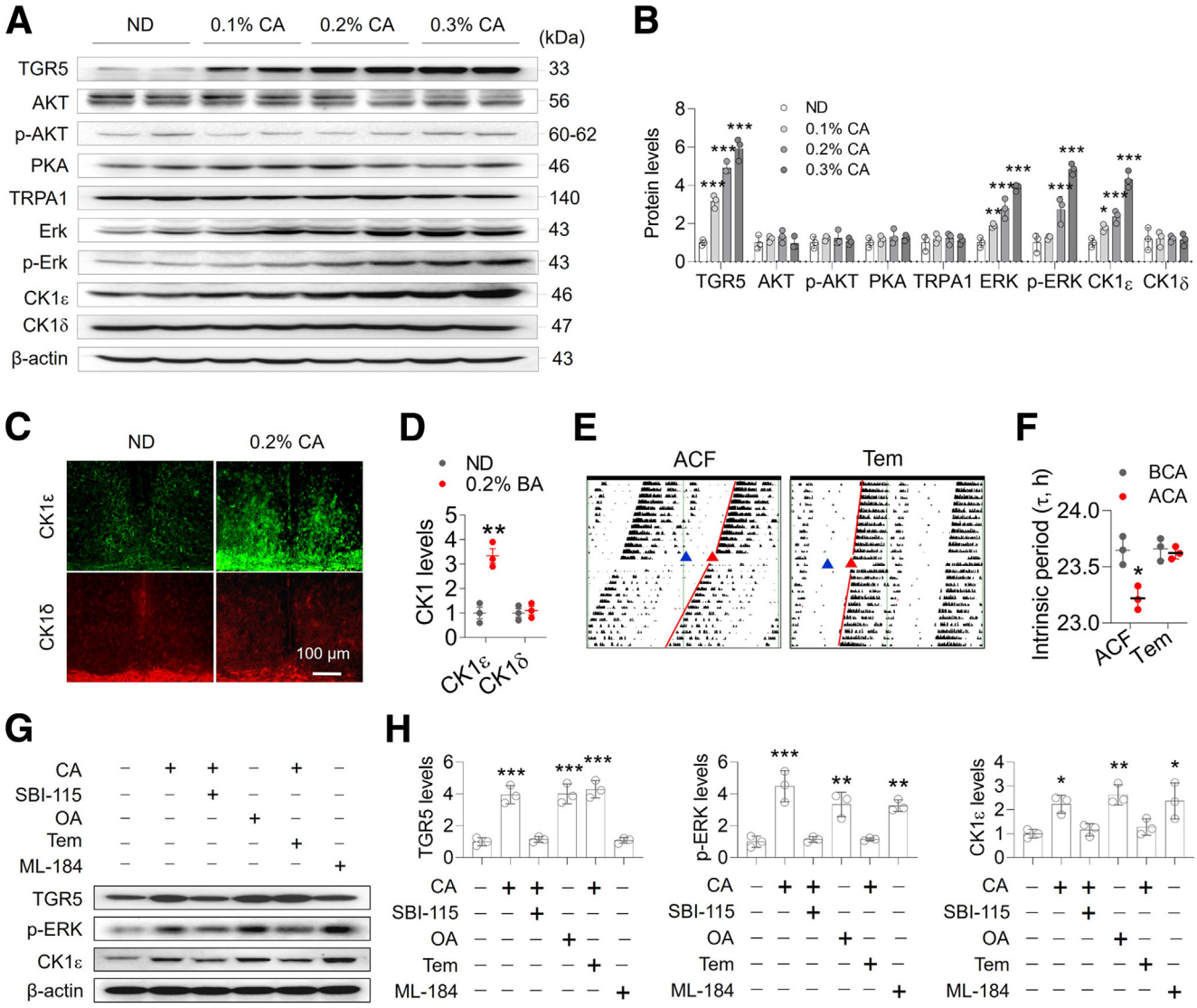

Figure 8. Erk and CK1ε mediate the CA-induced changes downstream of TGR5. Representative immunoblotting (*A*) and quantitation (*B*) of TGR5, AKT, p-AKT, cAMP, TRPA1, ERK, p-ERK, CK1ε, and CK1δ in the SCN of mice fed with increasing amount of CA (0.1%, 0.2%, 0.3%) for 1 week. Mean ± SEM, 2-way ANOVA, Tukey's multiple comparisons test, $^{*}P < .05$; $^{**}P < .01$; $^{***}P < .001$ vs ND, N = 3. Immunofluorescent staining (*C*) and semi-quantification (*D*) of CK1ε and CK1δ in the SCN of mice fed with ND or 0.2% CA diet for 1 week. *Green*, CK1ε; *red*, CK1δ. Mean ± SEM, paired 2-tailed *t*-test, $^{**}P < .01$ vs ND, N = 3. Representative wheel-running actograms (*E*) and intrinsic period (*F*) of mice injected with 0.2 μmoL temuterkib (Tem) or ACF. *Blue triangles* indicate the injection time of Tem, *red triangles* denote the beginning time of 0.2% CA diet. Mean ± SEM, paired 2-tailed *t*-test, $^{*}P < .05$ ACA (after CA diet) vs BCA (before CA diet), N = 3. Representative immunoblots (*G*) and quantitation (*H*) of TGR5, p-ERK, and CK1ε of the SCN from the mice injected with CA, SBI-115 (TGR5 antagonist), OA, Tem (Erk antagonist), and ML-184 (Erk agonist). Mean ± SEM, 1-way ANOVA, Tukey's multiple comparisons test, $^{*}P < .05$; $^{**}P < .01$; $^{***}P < .001$ vs the control group, N = 3

transmitted from the retina to the ventrolateral region of SCN via the retinohypothalamic tract, and the ventrolateral region of SCN mainly contains GRP neurons and VIP neurons.[40] Light signal induces acute expression of *Per1/2* and further promotes releasing of GRP and VIP from the ventrolateral region, which reach the dorsomedial region of SCN to deliver resetting signal and trigger the resynchronization process.[35] We show here that Tgr5 is mainly distributed in the GRP-containing neurons of SCN, and CA disrupts the light-induced synchronizing signals via Per2 and GRP. These findings explain why cholemic mice could not follow the normal LD environment and why the light-induced phase shift was blunted. The shorter sleep duration would result in accumulated sleep debt and increase the pressure of Process S in the patients with CLD. The failure of entrainment to external LD cycle would further cause the misalignment of Process S with Process C (Graphic Abstract). Immunohistochemistry showed that Tgr5 was also expressed in other

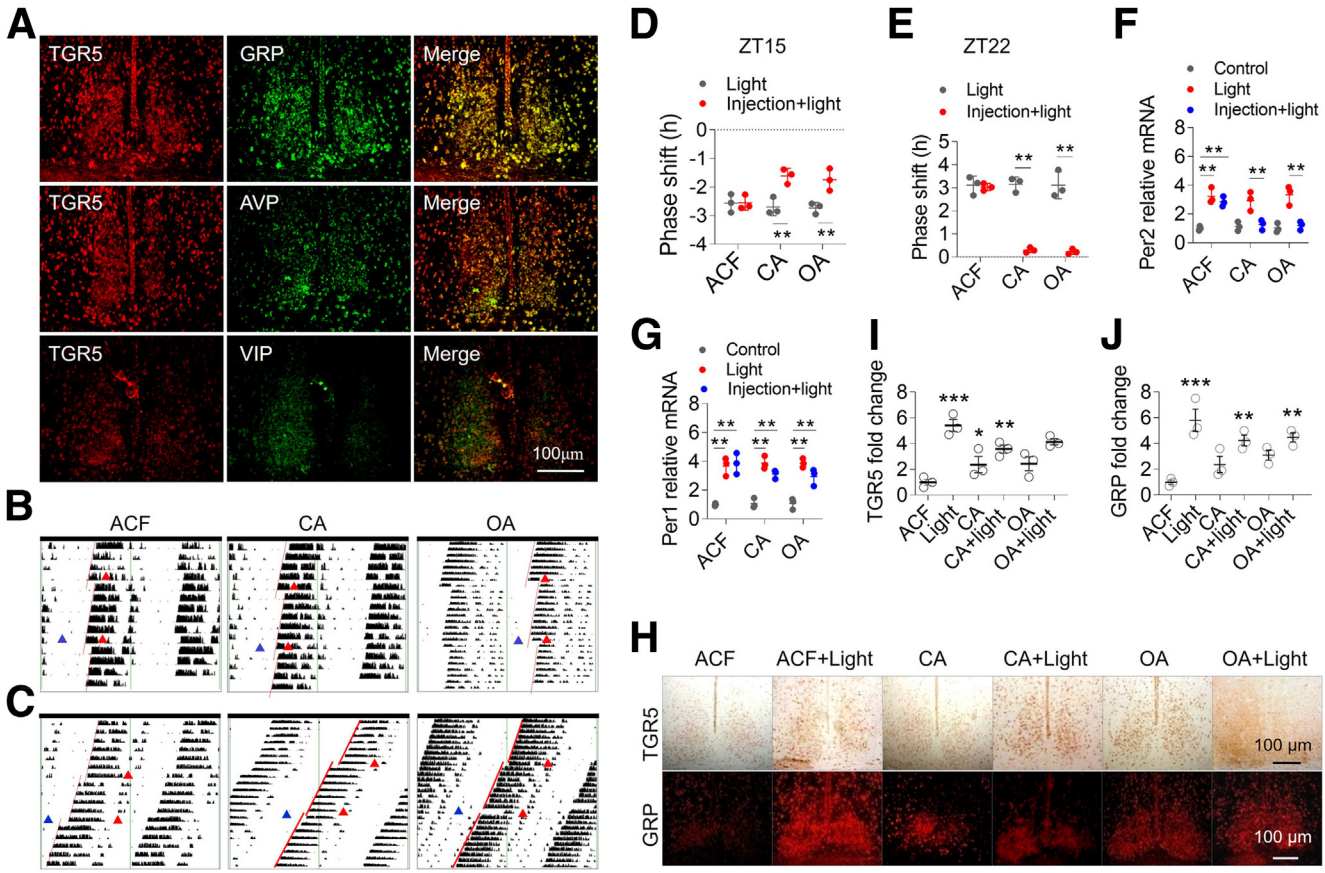

Figure 9. Light entrainment response is blunted in CA-treated mice. (*A*) Immunofluorescent staining showing double-labeling of TGR5 and GRP, TGR5 and AVP, and TGR5 and VIP. Note the co-localization (*yellow*) of TGR5 with GRP but not AVP and VIP in the merged images. (*B*) Representative actograms of the mice running under DD condition showing the phase delay effect of 30-min light pulse (200 lux) given at ZT15 after 10 nmoL of CA, OA or ACF was preinjected into the SCN at ZT6. (*C*) Representative actograms of the mice running under DD condition showing the phase advance effect of 30-min light pulse (200 lux) given at ZT22 after 10 nmoL of CA or OA or ACF was preinjected into the SCN at ZT6. *Red triangles* indicate the beginning time of light exposure, *blue triangles* denote the time (ZT6) of 10 nmol CA, 10 nmoL OA or ACF injection into the SCN. Phase delay (*D*), phase advance (*E*), and mRNA levels of *Per2* (*F*) of mice treated with light pulse or light pulse plus CA, OA, or ACF injection into the SCN. Mean ± SEM, 2-way ANOVA, Tukey's multiple comparisons test, $^{**}P < .01$ vs light or control, N = 3. (*G*) mRNA levels of *Per1* in the SCN after light pulse or light pulse plus CA or OA injection into the SCN. Mean ± SEM, paired 2-tailed *t*-test, $^{**}P < .01$ vs control, N = 3. (*H*) Immunohistochemical and immunofluorescent staining of TGR5 and GRP in the SCN of the mice treated with light pulse or light plus CA or OA combination. (*I, J*) Quantitation of TGR5 and GRP showed in panel *H*. Mean ± SEM, 1-way ANOVA, Tukey's multiple comparisons test, $^{*}P < .05$; $^{**}P < .01$; $^{***}P < .001$ vs the ACF mice, N = 3.

regions of the SCN and the brain. Tgr5-BA signaling might provide additional regulation in these neurons.

Finally, 2 pharmacological agents, CHO and PF-670462, can reverse the CRSDs in cholemic mice. Traditionally, CHO has been used in the treatment of cholestasis and hyperlipidemia.[41] Our findings suggest that CHO could be a repurposed drug to treat CRSDs in patients with CLD. In fact, in addition to BA sequestrant, drugs targeting other aspects of BA metabolism were also used to treat pruritus, fatigue, and SDs in PBC. These include peroxisome proliferator-activated receptor agonist Seladelpar and ileal BA transporter inhibitor Linerixibat.[42,43] PF-670462, a potent and selective inhibitor of CK1ε/δ[44] that could lengthen the circadian period in SCN,[45] is currently in pre-clinical development. PF-670462 effectively restores the rest-activity rhythm of CA-fed mice and thus represents another promising candidate to treat CRSD.

In conclusion, our findings uncovered a novel role of BAs in circadian rhythm regulation and CRSDs in CLDs. Lowering blood BAs and enhancing Per2 stability represent promising strategies in future clinical studies to treat the CRSDs in patients with CLD.

Materials & Methods

Patient Study

A total of 60 patients with CLD were recruited from the Third People's Hospital of Taiyuan and enrolled into this study, who suffered from one of the following CLDs: HB (n = 19), HBC (n = 14), NALC (n = 15), and PBC (n = 12).

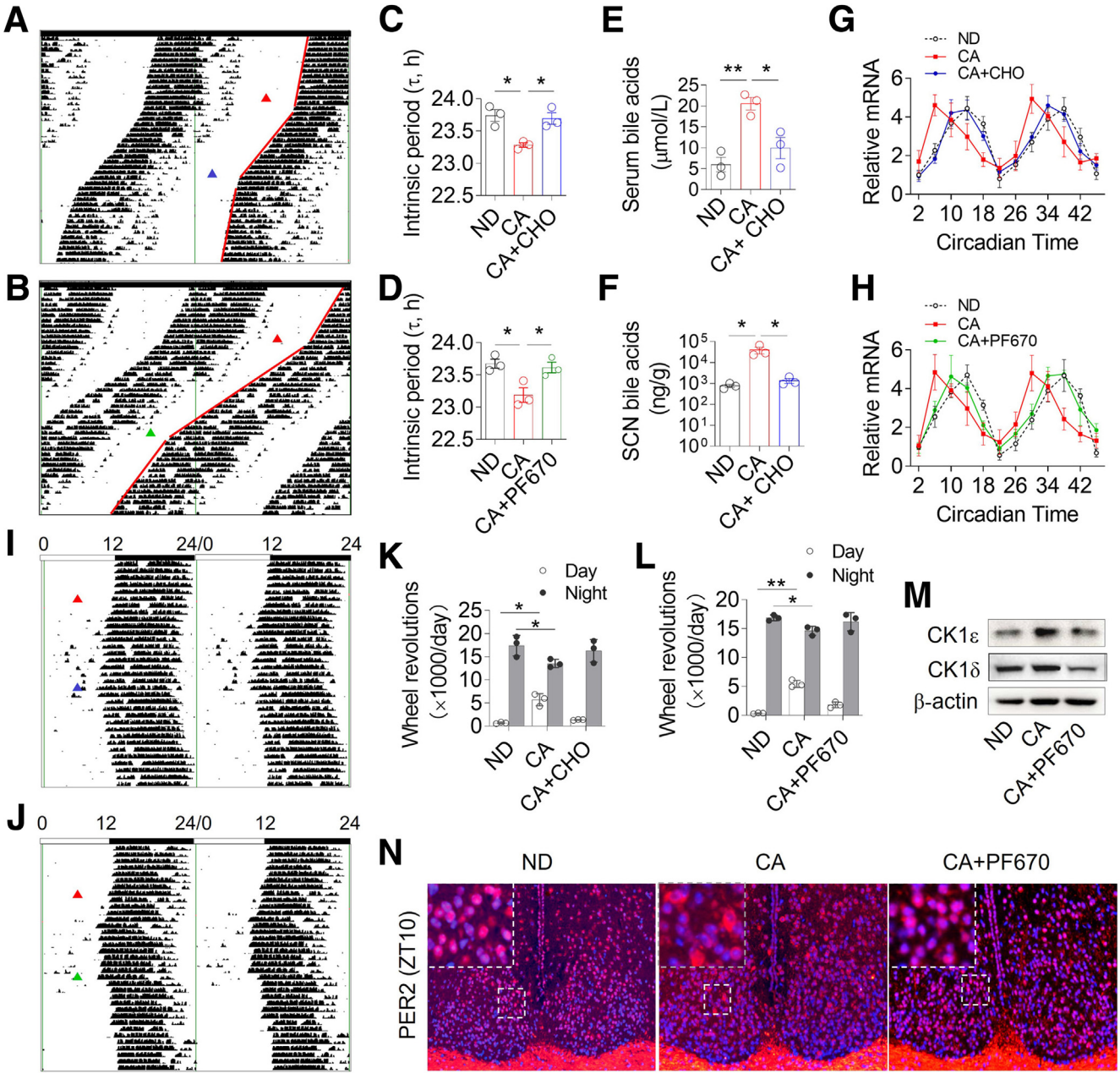

Figure 10. Rescue of CRSDs by BA sequestrant and CK1 inhibitor. Representative actograms showing the wheel-running activities of mice fed with ND, CA alone, CA+CHO (*A*), or treated with CA+PF-670462 (*B*) running under DD conditions, with their intrinsic periods shown in (*C, D*). *Red*, *blue* and *green triangles* denote the beginning time of CA diet, CHO supplementation, and the injection of PF670. Mean ± SEM, 1-way ANOVA, Tukey's multiple comparisons test, $^{*}P < .05$; $^{**}P < .01$; $^{***}P < .001$ vs ND or CA, N = 3. The serum (*E*) and SCN (*F*) levels of TBA in the mice given with ND, CA, or CA + CHO. Mean ± SEM, 1-way ANOVA, Tukey's multiple comparisons test, $^{*}P < .05$; $^{**}P < .01$; $^{***}P < .001$ vs ND, N = 3. Oscillation of *Per2* mRNA expression 1 week after the mice were given with CHO (*G*) or PF670 (*H*). Two circadian cycles are shown. Representative actograms of CA-fed mice running under LD12:12 condition and given with CHO (*I*) or PF670 (*J*). *Red*, *blue*, and *green triangles* denote the beginning time of CA diet, CHO supplementation and PF670 injection. Wheel revolution of the mice given with ND, CA, or CA + CHO (*K*) or CA + PF670 (*L*). Mean ± SEM, 2-way ANOVA, Tukey's multiple comparisons test, $^{*}P < .05$; $^{**}P < .01$ vs ND, N = 3. (*M*) Immunoblots of CK1ε and CK1δ in the SCN of mice given with ND, CA, or CA + PF670. (*N*) Immunofluorescent staining of Per2 in the SCN of mice treated with ND, CA, or CA + PF670 for 1 week under DD conditions. *Insets* show enlargements of the smaller framed areas. N = 3.

The participant demographics are shown in Table 1. We did not include any patient diagnosed with late stages of cirrhosis (III, IV), HE, and complications that would affect sleep or circadian rhythm, including heart diseases (New York Hearth Association Class III–IV), diabetes, neurodegenerative disease, stroke, long-term alcoholism, and use of

psychotropic drugs or opioids. All human studies were conducted following the Declaration of Helsinki Principles and the Guideline issued by the Ethics Committee of Taiyuan Third People's Hospital (Approval No.: 2023-21). All participants signed the informed consent form.

The sleep-wake cycle of patients with CLD was monitored using actigraphic watch equipped with ActiGraph GT3X+ accelerometer (ActiGraph). Patients were instructed to wear the watch for 7 consecutive days to measure their sleep parameters. The ActiLife 6 software (ActiGraph) was used to analyze the actigraphic parameters, including sleep onset time, out-bed time, TST, WASO, and SFI. Sleep onset indicated the first minute at which the algorithm scored "asleep." WASO was defined as the total numbers of minutes that the subject was awake after sleep onset. SFI was defined as the sum of the movement index (MI) and the fragmentation index (FI). MI was the percentage of epochs with y-axis counts >0 in the sleep period, whereas FI was the percentage of 1-min periods of sleep vs all periods of sleep during the sleep period. These parameters were used to evaluate sleep duration and quality. Blood biochemistry tests, including alanine aminotransferase, aspartate aminotransferase, total BAs, bilirubin, albumin, plasma D-dimer, plasma prothrombin time, creatinine, and hemoglobin, were carried out by the Department of Laboratory Medicine, Third People's Hospital of Taiyuan.

Animal Experiments: Chow and BDL

Male C57BL/6J mice, age 5 to 6 weeks and body weight 18 to 20 grams, were purchased from the Experimental Animal Center, Shanxi Medical University. All animals were individually housed in cages each equipped with a running wheel, and all the cages were placed in a light- and temperature-controlled (25 ± 1 °C) room with chow and water provided without restriction. The animal experiment protocol was approved by the Bioethical Committee of Shanxi Medical University (Approval No.: CIRP-IACUC-(R) 2019012) and was conducted in compliance with the Guide for the Care and Use of Laboratory Animals (NIH Publication No. 85-23, Revised 1996).

The mouse model of cholemia was induced by feeding with BAs or by common BDL. Specifically, mice were fed with normal chow supplemented with 0.2% (w/w) of CA, CDCA, LCA, and UDCA. The BA-containing chows were prepared by Beijing Huafukang Biotechnology Co LTD. BDL was performed based on a classical protocol and a recent modification for mice.[46,47] The mice are subjected to double ligation of the common bile duct followed by a section of the bile duct between the ligatures. Specifically, the mice received 60 μg/kg body weight of buprenorphine before the surgery. Midline laparotomy was performed under isoflurane anesthesia. The bile duct was isolated from the surrounding tissues, and silk ligatures were tied at proximal and distal end to the liver hilus. Finally, the bile duct was resected between the 2 ligatures. In the sham-operated animals, the bile duct was only isolated but not ligated. The BDL and sham-operated animals were sacrificed 7 days after surgery, and the plasma and tissues were harvested for further experiments.

EEG/EMG Recordings and Sleep Analysis

For EEG/EMG monitoring, C57BL/6J Mice were deeply anesthetized with isoflurane (1%–3%) and fixed to a mouse stereotaxic apparatus (RWD Life Science). The skull bone was exposed after incision of the skin. Two symmetrical holes (diameter, 0.7 mm) were made perpendicularly to the skull with a skull drill (RWD Life Science) at the sites (anteroposterior, A/P: 1.8 mm; medio-lateral, M/L: ±1.5 mm). Two EEG electrodes were screwed into the skull from the holes separately, and a reference electrode was screwed into the skull at the site (A/P: −2.0 mm, M/L: 1.5 mm), with 2 flexible wires for EMG recording inserted in the neck muscle. The electrode base was then fixed on the mouse skull with dental cement. For postsurgical recovery, the mice were placed under the LD 12:12 circumstance for 1 week and then in the recording chamber on a swivel mounted system from Shike Biotechnology for another 2 days of adaptation to allow them to move freely in their cage. Then EEG/EMG signal was then recorded continuously for consecutive 24-hour periods.

EEG/EMG signals were amplified using Powerlab PL15T02 (AD Instruments), filtered (EEG: 0.5–300 Hz; EMG: 30–300 Hz) and digitized at a sampling rate of 1000 Hz. The data were finally analyzed by Sleep Pro software (Pinnacle Technology) for the scoring of sleep states in 10-second epochs during the 24-hour recording. The sleep states include wake, NREM sleep, and REM sleep, using the following criteria: (1) wake: active behavior accompanied by desynchronized EEG of low amplitude; (2) NREM sleep: more synchronized EEG, higher in amplitude, with particularly notable power in the delta (0.5−4.0 Hz) band, and low EMG activity; and (3) REM sleep: small amplitude EEG, particularly notable power in the theta (5.5−8.5 Hz) band, and lower EMG activity.

Locomotor Wheel-running Experiments

The wheel-running experiments were conducted as previously decribed.[48] Animals were subjected to voluntary wheel running under the LD 12:12 circumstance for 7 days before any experiment. Then one-half of the mice were kept in the LD 12:12 circumstance, and the other one-half of mice were released into constant darkness (DD). All mice were continuously monitored for 1 month, and locomotor activity signals were acquired by the VitalView Data Acquisition System (Mini-Mitter). Data were analyzed by the ActiView Biological Rhythm Analysis software (Mini-Mitter). The recorded circadian variation of rest and activity was used to approximate the sleep-wake rhythm of the mice and deduce their circadian periods. To measure the phase-delay effect, a light pulse was given at CT15 after the mice were treated with CA or OA.

Under LD 12:12 condition, the rest-activity rhythms were monitored before and after the mice were fed with increasing amount of CA, 0.1%, 0.2%, 0.3% (w/w) and exposed to light environment of different lumens (ie, different intensities [100, 200, and 300 lux]). To measure the effects of CA and OA on light entrainment and "jet-lag"

phase shift, the mice were subjected to an 8-hour advance from the conventional LD 12:12 schedule, and the locomotor activities were recorded during the re-entrained days. For therapeutic experiments, 3% (w/w) CHO (MCE, HY-104081) was added to the diet, and PF-670462 dihydrochloride (MCE, HY-15490) was subcutaneously injected.

Intracephalic Injection and Transfection in Mice in vivo

Intracephalic injection was carried out under the normal light (200 lux) or under DD (dim red light, <4 lux) condition after the mice adapted to the voluntary wheel-running environment for at least 2 weeks. Animals were anesthetized with 20% urethane hydrate (1.3 g/kg body weight, intraperitoneal) and placed on a stereotaxic apparatus (RWD Life Science). The skull bone was exposed after incision of the skin. Two symmetrical holes (diameter 1 mm) were made perpendicularly to the skull with a skull drill (RWD Life Science) at the injection site (A/P: −0.46 mm; M/L: 0.2 mm). A glass micropipette was attached to a 10-μL syringe and then slowly and vertically inserted into the hole (depth 5.6 mm from the skull surface) to reach the left and right SCN.

For CA and OA microinjection, 1 nmoL or 10 nmoL of CA (Sigma, C1129) and OA (MCE, HY-N0156) was prepared in 4 μL of ACF and injected into the SCN with 2 μL into each side at a rate of 200 nL/min using a microinjection pump (RWD Life Science). For RNAi of *Tgr5*, the recombinant AAV encoding the short hairpin RNAs (shRNAs) against the mouse *Tgr5* was co-injected into the SCN with a recombinant AAV encoding *EGFP* (pHBAAV-U6-mGpbar1-MCS-CMV-EGFP), which served as a positive control for neuron infection. 1.5 μL of 2 recombinant AAVs (1.0×10^{12} μg/mL) were mixed and injected into each side of the SCN at the abovementioned rate. The AAV encoding the shRNAs against *Tgr5* was prepared by Hanbio company, and the shRNA sequences were as follows: Top strand: 5′-AATTCG GAACTCTGTTATCGCTCATCTCATTTCAAGAGAATGAGATGAG CGATAACAGAGTTCCTTTTTTG-3′; Bottom strand: 5′-GATC CAAAAAAGGAACTCTGTTATCGCTCATCTCATTCTCTTGAAATGA GATGAGCGATAACAGAGTTCCG-3′.

After microinjection, the glass micropipette was kept inside for 10 minutes and then slowly withdrawn over 5 minutes. After removing the glass micropipette, the burr hole was sealed with bone cement, and mice were put back to the cage after they were fully awake. The mice usually resumed normal activities within 12 hours after surgery and continued voluntary wheel running afterwards.

BA Extraction and Liquid Chromatography-mass Spectrometry Analysis

Venous EDTA-blood was drawn from the patients with CLD and centrifuged 3000 × g at 4 °C for 10 minutes to produce plasma. Mouse retro-orbital blood was collected and allowed to sit 30 to 60 minutes to produce serum. Human plasma, mouse serum, and mouse SCN tissues, which were dissected from the mouse brain, were snap-frozen in liquid nitrogen. Approximately 100 mg of SCN or 100 μL plasma or serum was homogenized in or mixed with 200 μL of 50% methanol. 300 μL of homogenate was spiked with 20 μL internal standard. Then 2 mL of ice-cold alkaline ACN was added, and the samples were vortexed, shaken continuously for 1 hour, and centrifuged at 11,000 g for 10 minutes. The supernatant was aspirated and precipitant was extracted with another 1 mL of ice-cold alkaline ACN. Supernatants from the 2 extraction steps were pooled, evaporated, and reconstituted in 100 μL of 50% MeOH. The samples were applied to ultra high-pressure liquid chromatography system coupled with a Q-Exactive orbitrap mass spectrometer (Thermo Fisher).

BA identification was performed by comparing accuracy of m/z value (<25 ppm), and tandem mass spectrometry (MS/MS) with an in-house database established with available standards. The 7-fold cross-validation and response permutation testing were used to evaluate the robustness of the model. The variable importance in the projection value of each variable in the orthogonal partial least squares discriminant analysis (OPLS-DA) model was calculated to indicate its contribution to the classification. BA with the VIP value >1 was further applied to Student's *t*-test at univariate level to measure the significance of each BA; the *P* values less than .05 were considered as statistically significant.

Cell Culture, Chemicals, and Reagents

Mouse embryonic fibroblast NIH3T3 cells were purchased from China Center for Type Culture Collection, cultured in Dulbecco modified Eagle medium (DMEM; Hyclone) supplemented with 10% fetal bovine serum (FBS; Hyclone), 100 U/mL penicillin, and 100 μg/mL streptomycin, and maintained at 37 °C in a water-saturated chamber containing 5% CO_2. For serum shock experiment, cells were cultured in 24-well plates for a day before the medium was changed with DMEM supplemented with 50% horse serum (Procell) at the time 0. Two hours after the serum shock was applied, the high serum-containing medium was replaced with a serum-free DMEM. Cells were then harvested every 4 hours, and 13 samples in total were collected for immunoblotting or immunofluorescence analysis. Reagents used in cell culture experiment included SBI-115 (MCE, HY-111534) at 10 μM, temuterkib (MCE, HY-101494) at 5 μM, ML-184 (MCE, HY-116461) at 1 μM, OA (MCE, HY-N0156) at 1 μM, and CA (Sigma, C1129) at 1 μM. Other chemicals and reagents were from Sigma unless otherwise stated.

For overexpression experiment, the cDNAs encoding mouse *Per2*, *Per1*, *Clock*, *Bmal1,* and *Cry1* were subcloned in pcDNA3.1 constructs, and 2 μg of DNA were mixed with lipofectamine 2000 (Life Technologies) and transfected into the NIH3T3 cells seeded at 1.25×10^5 cells per well in 6 well plates. For siRNA transfection experiment, the NIH3T3 cells were seeded at 1.25×10^5 cells per well in 6 well plates and transfected with lipofectamine 2000 (Life Technologies) and 150 pmoL of siRNAs targeting the mouse clock genes. Cells were harvested 48 hours after transfection for immunoblotting analysis. The siRNA sequences

are as follows. *Per2*: Sense, 5′-GGAAGAUAUCUU UCAUCAUTT-3′; Anti-sense, 5′-AUGAUGAAAGAUAUCUUC CTG-33; *Per1*: Sense, 5′-GCUCUUCAUUGAAUCUCGGTT-3′; Anti-sense, 5′-CCGAGAUUCAAUGAAGAGCTG-3′; *Clock*: sense, 5′-CCUUAGUAAUGAAGAGUUUTT-33; Anti-sense, 5′-AAACU CUUCAUUACUAAGGTT-3′; *Bmal1*: Sense, 5′-GCAACAGG CCUUCAGUAAATT-3′; Anti-sense, 5′-UUUACUGAAGGCCU GUUGCTT-3′; negative control siRNA: sense, 5′-UUCUCC GAACGUGUCACGUTT-3C; Anti-sense, 5′-ACGUGACACGUUC GGAGAATT-3C. For *Cry1*, we purchased siRNA against mouse *Cry1* (sc-44835) from Santa Cruz Biotechnology and performed transfection following the manufacturer's instructions.

Immunofluorescent and Immunohistochemical Staining

Immunofluorescent staining was performed in mouse SCN paraffin sections and NIH/3T3 cells. Cells or tissues were fixed with 4% formalin in phosphate-buffered saline (PBS) for 10 minutes, followed by permeabilization with 0.5% Triton X-100 for 5 minutes and blocking by 1% bovine serum albumin (BSA) for 30 minutes. Mice brains were fixed with 4% formalin. SCN was carefully dissected and embedded in paraffin. Five-μm SCN sections were cut with a microtome. Sections were deparaffinized, rehydrated, permeabilized with 0.5% Triton X-100 for 30 minutes, and blocked with 1% BSA for 60 minutes. Cells or SCN sections were incubated with primary antibody overnight at 4 °C. The primary antibodies were anti-PER2 (LSBio, Ls-c148562), anti-CK1ε (Proteinteck, 11230), anti-GRP (Solarbio, K004476P), anti-VIP (Abcam, ab8556), anti-AVP (Abcam, ab272726), and anti-TGR5 (Abcam, ab72608). After incubation with primary antibodies and washing with PBS for 3 times, the cells or sections were incubated with secondary antibodies labeled with Alexa Fluor 488 (ZSGB-bio, ZF-0511) or Alexa Fluor 594 (ZSGB-bio, ZF-0516) for 1 hour at room temperature and then were mounted on slides with mounting medium containing DAPI (ZSGB-bio, ZLI-9557). Fluorescent images were captured using a phase contrast microscope or inverted fluorescent microscope (Nikon).

Immunoblotting. The mouse SCN tissues were lysed in RIPA buffer supplemented with protease inhibitors, and total proteins were extracted. To obtain enough proteins, SCN of five animals from the same treatment group were pooled together. The protein concentration was determined using a bicinchoninic acid kit (Solarbio, PC0020) following manufacturer's instruction. Fifty micrograms of total protein were separated by 10% SDS-polyacrylamide gels. After electrophoretic transfer, the PVDF membrane (Millipore) was blocked with 5% BSA for 1 hour at room temperature and incubated overnight at 4 °C with the following primary antibodies: anti-CLOCK (1:1000, Abcam, ab134165), anti-BMAL1 (1:500, Abcam, ab134165), anti-CRY1 (1:1000, Abcam, ab104736), anti-PER1 (1:1000, Abcam, ab3443), anti-PER2 (1:300, LSBio, Ls-c148562), anti-phospho-PER2 (1:1000, LSBio, Ls-c381359), anti-Ubiquitin (1:1000, Proteintech, 10201-1-AP), anti-ERK1/2 (1:300, Proteintech, 16443-1-AP), anti-phospho-ERK1/2 (1:300, Proteintech, 28733-1-AP), anti-TRPA1 (1:500, Proteintech, 19124-1-AP), anti-CK1ε (1:500, Proteintech, 11230-1-AP), anti-CK1δ (1:500, Proteintech, 14388-1-AP), anti-TGR5 1(1:2000, Abcam, ab72608), anti-AKT (1:1000, Proteintech, 10176-2-AP), anti-PKA (1:1000, Proteintech, 55382-1-AP), anti-phospho-AKT (1:500, Proteintech, 66444-1-AP), and anti-β-actin (1:5000, Bioworld, AP0060). The secondary antibodies were all from ZSGB-Bio Company. Immunolabeled proteins were visualized with an ECL reagent (ZSGB-Bio) and were quantified by densitometry using Image J software.

RT-qPCR

The mRNA levels of clock genes in the SCN were detected using RT-qPCR. Mice were decapitated under dim red light (<4 lux), and SCN tissues were immediately harvested at CT2, CT6, CT10, CT14, CT18, and CT22 and stored in liquid nitrogen before use. Total RNAs were extracted in Trizol (Invitrogen), and single-strand cDNA was prepared from 2 μg total RNA by reverse transcription (Prime ScriptTMRT reagent kit, RR047A, Takara). qPCR was performed using the Step One PlusTM Real-time PCR system (Applied Biosystems) with SYBR Green PCR Master Mix (TB Green Premix Ex TaqTMII) and primers specific for mouse *Clock*, *Bmal1*, *Per1*, *Per2*, *Tgr5,* and *β-actin*. Briefly, both *β-actin* (used as a loading control) and the target gene from the same sample were amplified in duplicate tubes for each assay. The mRNA levels of each gene were calculated with reference to the relative standard curve and expressed as relative change over the β-actin control. The primers were designed using the Primer Express V1.5 software (Applied Biosystems). The sequence of forward and reverse primers (separated by semicolon) of the mouse genes investigated in this study were as follows. *Clock*: forward, 5′-TTG CTCCACGGGAATCCTT-3′; reverse, 5′-GGAGGG AAAGTGCTC TGTTGTAG-3′; *Bmal1*: forward, 5′-TGGCCGCTGTAGACACTA CATT-3′; reverse, 5′-CTCTATCCAGTAAGCTTCACAGACTGTAA-3′; *Per1*: forward, 5′-TCGAAACCAGGACACCTTCTCT-3′; reverse, 5′-GGGCACCCCGA AACACA -3′; *Per2*: forward, 5′-ATGCTCGC-CATCCACAAGA-3′; reverse, 5′-GCGGAA TCGAATGGGAGAAT-3′; *Tgr5*: forward, 5′-GGCAAGCCTCATC ATCACC-3′; reverse, 5′-AAGTTGGGAGCCAAGTAGACG-3′; *Fxr*: forward, 5′- CC AACCT GGGTTTCTACCC-3′; reverse, 5′-CACACAGCTCATCCCCTTT-3′; *Pxr*: forward, 5′-GAGGCGTGGCAGACTATGC-3′; reverse, 5′-CTTGTACTCCG TCAGCGTGA- 3′; *Vdr*: forward, 5′-GATGC CCACCACAAGACCTA-3′; reverse, 5′- CGGTTCCATCAT GTCCAGTG-3′; *β-actin*: forward, 5′-TCAAGATCATTGCT CCTCCTGAG; reverse, 5′ -CTGCTTGCTGATCCACATCTG; *TNF-α:* forward, 5′-C CCACGTCGTAGCAAACCAC-3′; reverse,5′-GCAGCCTTGTCCCTTGAAGA -3′; *IL-1β*: forward, 5′-TGACGGACCCCAAAAGATGA-3′; reverse, 5′-AAAGACACA GGTAGCTGCCA-3′; *IL-10*: forward, 5′-ATAACTGCACCCA CTTCCCA-3′; reverse, 5′-GGGCATCACTTCTACCAGGT-3′; *IL-6*: forward, 5′-ACAACCACGG CCTTCCCTACTT-3′; reverse, 5′-CACGATTTCCCAGAGAACATGTG-3′.

Statistical Analysis

Statistical analyses were performed using SPSS software (version 22.0) and GraphPad Prism 8.4.3 software.

Statistical differences were determined with multivariate linear regression analysis, paired and unpaired Student's *t*-tests, 1-way analysis of variance (ANOVA) or 2-way ANOVA followed by Tukey's multiple comparisons test. All data are expressed as mean ± standard error of the mean (SEM): $^{***}P < .001$; $^{**}P < .01$; $^{*}P < .05$; ns = not significant. The statistical analyses are described in details in each figure legend.

References

1. Evon D, Stewart P, Amador J, et al. A comprehensive assessment of patient reported symptom burden, medical comorbidities, and functional well-being in patients initiating direct acting antiviral therapy for chronic hepatitis C: results from a large US multi-center observational study. PLoS One 2018;13:e0196908.
2. Heeren M, Sojref F, Schuppner R, et al. Active at night, sleepy all day–sleep disturbances in patients with hepatitis C virus infection. J Hepatol 2014;60:732–740.
3. Carlson M, Hilsabeck R, Barakat F, Perry W. Role of sleep disturbance in chronic hepatitis C infection. Curr Hepat Rep 2010;9:25–29.
4. Um Y, Chang Y, Jung H, et al. Sleep duration, sleep quality, and the development of nonalcoholic fatty liver disease: a cohort study. Clin Transl Gastroenterol 2021;12:e00417.
5. Mostacci B, Ferlisi M, Baldi Antognini A, et al. Sleep disturbance and daytime sleepiness in patients with cirrhosis: a case control study. Neurol Sci 2008;29:237–240.
6. Kim M, Liotta E, Maas M, et al. Rest-activity rhythm disturbance in liver cirrhosis and association with cognitive impairment. Sleep 2021;44:zsaa288.
7. Swain M, Jones D. Fatigue in chronic liver disease: new insights and therapeutic approaches. Liver Int 2019;39:6–19.
8. Montagnese S, Nsemi L, Cazzagon N, et al. Sleep-wake profiles in patients with primary biliary cirrhosis. Liver Int 2013;33:203–209.
9. Shah NM, Malhotra AM, Kaltsakas G. Sleep disorder in patients with chronic liver disease: a narrative review. J Thorac Dis 2020;12:S248–S260.
10. Plotogea OM, Ilie M, Bungau S, Chiotoroiu AL, Stanescu AMA, Diaconu CC. Comprehensive overview of sleep disorders in patients with chronic liver disease. Brain Sci 2021;11:142.
11. Wijarnpreecha K, Thongprayoon C, Panjawatanan P, Ungprasert P. Short sleep duration and risk of nonalcoholic fatty liver disease: a systematic review and meta-analysis. J Gastroenterol Hepatol 2016;31:1802–1807.
12. Borbély A. The two-process model of sleep regulation: beginnings and outlook. J Sleep Res 2022;31:e13598.
13. Borbély AA. A two-process model of sleep regulation. Hum Neurobiol 1982;1:195–204.
14. Takahashi J. Transcriptional architecture of the mammalian circadian clock. Nat Rev Genet 2017;18:164–179.
15. Masuda S, Narasimamurthy R, Yoshitane H, Kim J, Fukada Y, Virshup D. Mutation of a PER2 phosphodegron perturbs the circadian phosphoswitch. Proc Natl Acad Sci U S A 2020;117:10888–10896.
16. Tamanini F, Yagita K, Okamura H, van der Horst G. Nucleocytoplasmic shuttling of clock proteins. Meth Enzymol 2005;393:418–435.
17. Narasimamurthy R, Hunt S, Lu Y, et al. CK1δ/ε protein kinase primes the PER2 circadian phosphoswitch. Proc Natl Acad Sci U S A 2018;115:5986–5991.
18. Francisco J, Virshup D. Casein kinase 1 and human disease: insights from the circadian phosphoswitch. Front Mol Biosci 2022;9:911764.
19. Gallego M, Virshup D. Post-translational modifications regulate the ticking of the circadian clock. Nat Rev Mol Cell Biol 2007;8:139–148.
20. Hattar S, Liao H, Takao M, Berson D, Yau K. Melanopsin-containing retinal ganglion cells: architecture, projections, and intrinsic photosensitivity. Science 2002;295:1065–1070.
21. Kim M, Lee J, Duffy J. Circadian rhythm sleep disorders. J Clin Outcomes Manag 2013;20:513–528.
22. Farhat Z, Freedman ND, Sampson JN, et al. A prospective investigation of serum bile acids with risk of liver cancer, fatal liver disease, and biliary tract cancer. Hepatol Commun 2022;6:2391–2399.
23. Yu Z, Yang J, Xiang D, Li G, Liu D, Zhang C. Circadian rhythms and bile acid homeostasis: a comprehensive review. Chronobiol Int 2020;37:618–628.
24. Yang Y, Zhang J. Bile acid metabolism and circadian rhythms. Am J Physiol Gastrointest Liver Physiol 2020;319:G549–G563.
25. Panasiuk A, Tarasewicz M, Chodowiec A, Łokić A, Gan K. Biological rhythms of the liver. Clin Exp Hepatol 2024;10:1–8.
26. Ferrell JM, Chiang JY. Circadian rhythms in liver metabolism and disease. Acta Pharm Sin B 2015;5:113–122.
27. Wagner M, Fickert P. Drug therapies for chronic cholestatic liver diseases. Annu Rev Pharmacol Toxicol 2020;60:503–527.
28. Perez MJ, Briz O. Bile-acid-induced cell injury and protection. World J Gastroenterol 2009;15:1677–1689.
29. Reid KJ, Zee PC. Circadian rhythm disorders. Semin Neurol 2009;29:393–405.
30. Dhanda S, Sandhir R. Blood-brain barrier permeability is exacerbated in experimental model of hepatic encephalopathy via MMP-9 activation and downregulation of tight junction proteins. Mol Neurobiol 2018;55:3642–3659.
31. Quinn M, McMillin M, Galindo C, Frampton G, Pae HY, DeMorrow S. Bile acids permeabilize the blood brain barrier after bile duct ligation in rats via Rac1-dependent mechanisms. Dig Liver Dis 2014;46:527–534.
32. Watanabe M, Morimoto K, Houten SM, et al. Bile acid binding resin improves metabolic control through the induction of energy expenditure. PLoS One 2012;7:e38286.
33. Zhang Y, Hong JY, Rockwell CE, Copple BL, Jaeschke H, Klaassen CD. Effect of bile duct ligation on bile acid composition in mouse serum and liver. Liver Int 2012;32:58–69.
34. Hylemon P, Zhou H, Pandak W, Ren S, Gil G, Dent P. Bile acids as regulatory molecules. J Lipid Res 2009;50:1509–1520.
35. Piggins H, Antle M, Rusak B. Neuropeptides phase shift the mammalian circadian pacemaker. J Neurosci 1995;15:5612–5622.

36. Higashi T, Watanabe S, Tomaru K, et al. Unconjugated bile acids in rat brain: analytical method based on LC/ESI-MS/MS with chemical derivatization and estimation of their origin by comparison to serum levels. Steroids 2017;125:107–113.
37. Rodríguez V, Rivoira M, Marchionatti A, Pérez A, Tolosa de Talamoni N. Ursodeoxycholic and deoxycholic acids: a good and a bad bile acid for intestinal calcium absorption. Arch Biochem Biophys 2013;540:19–25.
38. Williams E, Chu C, DeMorrow S. A critical review of bile acids and their receptors in hepatic encephalopathy. Anal Biochem 2022;643:114436.
39. McMillin M, Frampton G, Tobin R, et al. TGR5 signaling reduces neuroinflammation during hepatic encephalopathy. J Neurochem 2015;135:565–576.
40. Karatsoreos IN, Yan L, LeSauter J, Silver R. Phenotype matters: identification of light-responsive cells in the mouse suprachiasmatic nucleus. J Neurosci 2004;24:68–75.
41. Maugeais C, Annema W, Blum D, Mary J, Tietge U. rHDL administration increases reverse cholesterol transport in mice, but is not additive on top of ezetimibe or cholestyramine treatment. Atherosclerosis 2013;229:94–101.
42. Kremer AE, Mayo MJ, Hirschfield G, et al. Seladelpar improved measures of pruritus, sleep, and fatigue and decreased serum bile acids in patients with primary biliary cholangitis. Liver Int 2022;42:112–123.
43. von Maltzahn R, Mayo MJ, Smith HT, et al. Relationship between pruritus and sleep in participants with primary biliary cholangitis in the Phase 2b GLIMMER trial. J Patient Rep Outcomes 2024;8:60.
44. Badura L, Swanson T, Adamowicz W, et al. An inhibitor of casein kinase I epsilon induces phase delays in circadian rhythms under free-running and entrained conditions. J Pharmacol Exp Ther 2007;322:730–738.
45. Meng Q, Maywood E, Bechtold D, et al. Entrainment of disrupted circadian behavior through inhibition of casein kinase 1 (CK1) enzymes. Proc Natl Acad Sci U S A 2010;107:15240–15245.
46. Kountouras J, Billing BH, Scheuer PJ. Prolonged bile duct obstruction: a new experimental model for cirrhosis in the rat. Br J Exp Pathol 1984;65:305–311.
47. Tag CG, Weiskirchen S, Hittatiya K, Tacke F, Tolba RH, Weiskirchen R. Induction of experimental obstructive cholestasis in mice. Lab Anim 2015;49:70–80.
48. Zhou L, Gao Q, Nie M, et al. Degeneration and energy shortage in the suprachiasmatic nucleus underlies the circadian rhythm disturbance in ApoE(-/-) mice: implications for Alzheimer's disease. Sci Rep 2016;6:36335.

Received February 15, 2024. Accepted December 4, 2024.

Correspondence
Address correspondence to: Ji-Min Cao, Key Laboratory of Cellular Physiology, Shanxi Medical University, Ministry of Education, Taiyuan, China. e-mail: caojimin@sxmu.edu.cn; or Lin Wang, Department of Physiology, Institute of Basic Medical Sciences, Chinese Academy of Medical Sciences, School of Basic Medicine, Peking Union Medical College, Beijing, China. e-mail: lin.wang@ibms.pumc.edu.cn.

CRediT Authorship Contributions
Lan Zhou (Conceptualization: Lead; Funding acquisition: Supporting; Project administration: Lead; Writing – original draft: Lead)
Min Yan (Data curation: Lead; Formal analysis: Equal; Methodology: Equal)
Qin Luo (Methodology: Supporting)
Wen Qiu (Methodology: Lead)
Yu-Ru Guo (Data curation: Supporting; Formal analysis: Equal)
Xiao-Qing Guo (Data curation: Supporting)
Hong-Bin Yu (Formal analysis: Lead)
Jing-Ru Huo (Data curation: Supporting)
Yan-Lin Feng (Software: Lead)
De-Ping Wang (Validation: Lead)
Teng Sun (Funding acquisition: Supporting; Investigation: Lead)
Kai-Fang Wang (Methodology: Supporting)
Jian-Yun Shi (Software: Equal)
Xuan Shang (Formal analysis: Equal)
Mei-Na Wu (Funding acquisition: Supporting; Validation: Supporting)
Lin Wang (Funding acquisition: Supporting; Writing – review & editing: Equal)
Ji-Min Cao (Funding acquisition: Lead; Writing – review & editing: Lead)

Conflicts of interest
The authors disclose no conflicts.

Funding
This study was supported by National Natural Science Foundation of China (31300967 to Lan Zhou, 31471126, 82170523 to Ji-Min Cao, 82271484 to Mei-Na Wu, 82170294 to Teng Sun, and 81550019 to Lin Wang), Applied Basic Research Program of Shanxi Province (201901D111189 to Lan Zhou, 20210302124302 to Kai-Fang Wang), Scientific Research Project of Shanxi Traditional Chinese Medicine Administration (2024ZYYB048 to Lan Zhou), and Shanxi "1331" Project Quality and Efficiency Improvement Plan (1331KFC to Ji-Min Cao).

Data Availability
The data, methods and materials are available upon request from the primary contact (Ji-Min Cao).